American Mineralogist, Volume 98, pages 1669–1687, 2013

Unlocking the secrets of Al-tobermorite in Roman seawater concrete†

Marie D. Jackson[1], Sejung R. Chae[1], Sean R. Mulcahy[2], Cagla Meral[1,6], Rae Taylor[1], Penghui Li[3], Abdul-Hamid Emwas[4], Juhyuk Moon[1], Seyoon Yoon[1,7], Gabriele Vola[5], Hans-Rudolf Wenk[2], and Paulo J.M. Monteiro[1,*]

[1]Department of Civil and Environmental Engineering, University of California, Berkeley, California 94720, U.S.A.
[2]Department of Earth and Planetary Science, University of California, Berkeley, California 94720, U.S.A.
[3]State Key Laboratory of Hydroscience and Engineering, Tsinghua University, Beijing, 100084, China
[4]King Abdullah University of Science and Technology, Thuwal, 23955-6900, Kingdom of Saudi Arabia
[5]Cimprogetti S.p.A., Via Pasubio 5, 24044, Dalmine, Italy
[6]Middle East Technical University, 06800, Ankara, Turkey
[7]School of Engineering, King's College, The University of Aberdeen, Aberdeen AB24 3UE, U.K.

Abstract

Ancient Roman syntheses of Al-tobermorite in a 2000-year-old concrete block submerged in the Bay of Pozzuoli (*Baianus Sinus*), near Naples, have unique aluminum-rich and silica-poor compositions relative to hydrothermal geological occurrences. In relict lime clasts, the crystals have calcium contents that are similar to ideal tobermorite, 33 to 35 wt%, but the low-silica contents, 39 to 40 wt%, reflect Al^{3+} substitution for Si^{4+} in Q^2(1Al), Q^3(1Al), and Q^3(2 Al) tetrahedral chain and branching sites. The Al-tobermorite has a double silicate chain structure with long chain lengths in the **b** [020] crystallographic direction, and wide interlayer spacing, 11.49 Å. Na^+ and K^+ partially balance Al^{3+} substitution for Si^{4+}. Poorly crystalline calcium-aluminum-silicate-hydrate (C-A-S-H) cementitious binder in the dissolved perimeter of relict lime clasts has Ca/(Si+Al) = 0.79, nearly identical to the Al-tobermorite, but nanoscale heterogeneities with aluminum in both tetrahedral and octahedral coordination. The concrete is about 45 vol% glassy zeolitic tuff and 55 vol% hydrated lime-volcanic ash mortar; lime formed <10 wt% of the mix. Trace element studies confirm that the pyroclastic rock comes from Flegrean Fields volcanic district, as described in ancient Roman texts. An adiabatic thermal model of the 10 m^2 by 5.7 m thick *Baianus Sinus* breakwater from heat evolved through hydration of lime and formation of C-A-S-H suggests maximum temperatures of 85 to 97 °C. Cooling to seawater temperatures occurred in two years. These elevated temperatures and the mineralizing effects of seawater and alkali- and alumina-rich volcanic ash appear to be critical to Al-tobermorite crystallization. The long-term stability of the Al-tobermorite provides a valuable context to improve future syntheses in innovative concretes with advanced properties using volcanic pozzolans.

Keywords: Al-tobermorite, ancient Roman concrete, bonding environments, volcanic pozzolan, thermal model

Introduction

Ancient Roman concrete, an extraordinarily durable, high-performance composite constructed from lime and pyroclastic rocks, provides a unique temporal window to address shortcomings in modern concrete longevity and environmental sustainability. The monuments of Rome, such as the Markets of Trajan (96 to 112 CE), are masterpieces of concrete engineering in architectural settings (Jackson et al. 2009, 2010; Brune and Perucchio 2012). Roman builders also constructed massive, enduring concrete structures in harbors along the central Italian coast (Fig. 1) and Mediterranean region (Oleson et al. 2004). They designed the seawater concrete so successfully that it "can neither be dissolved in the waves, nor by the power of water" [Vitruvius, *de Architectura,* 30 BCE (Appendix 1)]. The economic and military success of the expanding Roman empire depended on these ports, whose concrete structures have remained cohesive and intact while partially or wholly immersed in seawater for 2000 years. Romans mixed lime with pumiceous volcanic ash with seawater (Fig. 2) and packed this with decimeter-sized chunks of zeolitic tuff into underwater forms (Oleson et al. 2004). The ash, lime, and seawater reacted to produce poorly crystalline calcium-aluminum-silicate-hydrate (C-A-S-H) binder, intermingled with altered pumice and glass relicts in a complex cementitious matrix, which includes 11 Å Al-tobermorite (where Al^{3+} substitutes for Si^{4+}) in relict pebble lime clasts (Barnes and Scheetz 1991; Vola et al. 2011a; Stanislao et al. 2011; Jackson et al. 2012).

Preliminary studies of drill cores from piers, breakwaters, and fishponds along the central Italian coast (Fig. 1) indicate that the Al-tobermorite, identified through standard X-ray diffraction analysis, developed diagenetically in all the concretes while they were immersed in seawater (Jackson et al. 2012). It forms <10 vol% of most mortar fabrics. The longevity and cohesion of the seawater concrete apparently lies in Romans' selection of pozzo-

* E-mail: monteiro@ce.berkeley.edu

† Open access: Article available to all readers via GSW (http://ammin.geoscienceworld.org) and the MSA web site.

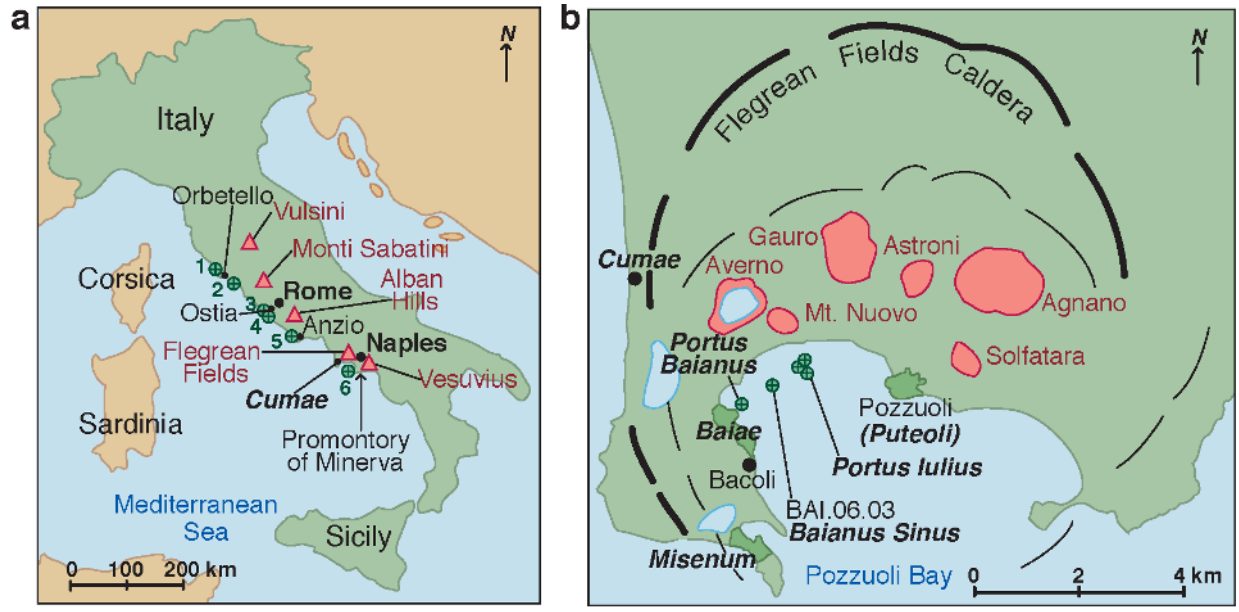

Figure 1. Ancient Roman seawater concrete harbor sites, central Italian coast, with Al-tobermorite in relict lime clasts, mid-first century BCE to first century CE. (**a**) Drill sites (green circles): 1 Santa Liberata, 2 *Portus Cosa*, 3 *Portus Claudius*, 4 *Portus Traianus*, 5 *Portus Neronis*, and 6 *Portus Baianus*, *Portus Iulius*, *and Baianus Sinus*, Volcanic districts (red triangles): (**b**) Flegrean Fields caldera and concrete drill cores, including *Baianus Sinus* BAI.2006.03 (after Orsi et al. 1996). Thick black lines: Campanian Ignimbrite caldera rim, thin black lines: Neapolitan Yellow tuff caldera rim; red areas: volcanic craters.

lanic pyroclastic rock, preparation of lime, installation techniques in immense piers and breakwaters—and the exceptional stability of the C-A-S-H binding phase. Mineralogical analyses of cores from 11 Roman harbors drilled by the ROMACONS project between 2002 and 2009 and descriptions of the concretes by Vitruvius, writing at about the same time as the construction of the Pozzuoli Bay harbors, and Pliny the Elder (*Naturalis Historia*, mid-first century CE) suggest that the pumiceous pozzolan (*pulvis*) originated from deposits surrounding the Bay of Naples (Fig. 1; Appendix 1) (Granger 1931; Rackham 1952; Oleson et al. 2004; Vola et al. 2011a; Stanislao et al. 2011; Jackson et al. 2012). A pozzolan is a siliceous and/or aluminous material, named after ash from Pozzuoli (Fig. 1), which reacts with lime or lime-based compounds in the presence of moisture at ordinary temperatures to produce compounds with cementitious properties (Massazza 2004). Flegrean Fields pozzolan, known in Italian as *pozzolana*, is mainly excavated from deposits of the Fondi di Baia and Bacoli volcanoes (near Bacoli; Fig. 1). It is composed of pumices, lithic fragments, K-feldspar, and a poorly consolidated altered vitric matrix with variable quantities of authigenic zeolites (de'Gennaro et al. 2000). The ash has mainly trachytic compositions on the total alkali-silica (TAS) classification diagram; glassy components may exceed 90% by volume (Stanislao et al. 2011; Fedele et al. 2011). The trace element provenance of the pumiceous component of the ancient ash pozzolan has not, however, been determined.

Conventional concretes typically consist of ordinary Portland cement (OPC), a crystalline, finely ground material derived from clinker calcined at 1450 °C, relatively inert sand and coarse aggregate, admixtures, and water that is pumped in a fluid state into forms (Taylor 1997). The concrete sets in a few hours, and hardens over a few weeks as OPC hydrates to form various compounds, mainly poorly crystalline calcium-silicate-hydrate (C-S-H), which bind the sand and coarse aggregates. Environmentally friendly concretes that partially replace kiln-fired Portland-type cement with supplemental cementitious materials, such as fly ash and blast furnace slag, and volcanic ash (Massazza 2004; Sun et al. 2006; Lothenbach et al. 2011), reduce fuel consumption and CO_2 emissions associated with production of Portland cement, while producing good ultimate strengths and longevity, even in tidal zones (Massazza 1985; Mehta 1990; Thomas et al. 2012). The poorly crystalline C-A-S-H binders of these concretes improve chemical stability relative to C-S-H, the "glue" of conventional Portland-type cement concretes, whose model basis is the ideal composition of tobermorite, $Ca_5Si_6H_2O_{18}{\cdot}4H_2O$ (Taylor 1992; Sun et al. 2006). C-A-S-H and 11 Å Al-tobermorite hold great potential as cementitious binders for high-performance concretes and concrete encapsulations of hazardous wastes (Komarneni and Roy 1983; Komarneni et al. 1987; Komarneni and Tsuji 1989; Tsuji et al. 1991), but the long-term performance of C-A-S-H is unknown and neither pure tobermorite nor Al-tobermorite occur in moist air-cured conventional concretes. Although laboratory syntheses of Al-tobermorite typically require high temperatures, 120 to 240 °C (Diamond 1966; Komarneni and Roy 1983; Komarneni and Tsuji 1989; Barnes and Scheetz 1991; Shaw et al. 2000; Sun et al. 2006; Houston et al. 2009), occasional syntheses have been achieved at 80 °C with amorphous silica and zeolites (Komarneni and Roy 1983; Komarneni et al. 1985), reactants similar to zeolitized alkali- and alumina-rich Flegrean ash pozzolan (de'Gennaro et al. 2000).

This study analyzes some of the mineralogical properties of C-A-S-H and Al-tobermorite in a concrete breakwater, or *pilae*, constructed in Pozzuoli Bay (*Baianus Sinus*) in first century BCE, now submerged under ~3.5 m of seawater. It integrates

interdisciplinary findings from mineral physics, geochemistry, engineering, and archaeological science to investigate why Roman builder's 2000-year-old natural experiment could produce crystalline Al-tobermorite but conventional concretes cannot. First, the occurrence of C-A-S-H and Al-tobermorite in relict lime clasts is described. Second, the volcanic provenance of the glassy tuff and pumiceous pozzolan is identified through trace element analyses. Third, the nanoscale bonding environments of Al^{3+} and Si^{4+} in Al-tobermorite and C-A-S-H are described with synchrotron-based scanning transmission soft X-ray microscopy (STXM) analysis and nuclear magnetic resonance (NMR) studies. These results provide an analytical framework to compare the compositions of Al-tobermorite syntheses from *Baianus Sinus* and *Portus Neronis,* the harbor concrete at Anzio (Fig. 1), with geologic Al-tobermorite {$[Ca_4(Si_{5.5}Al_{0.5}O_{17}H_2)]Ca_{0.2}\cdot Na_{0.1}\cdot 4H_2O$ (Taylor 1992)} from hydrothermal environments. The silica and alumina bonding environments of the C-A-S-H and Al-tobermorite are then compared with young laboratory syntheses. Next, the mix design of the *Baianus Sinus* concrete is determined as weight percent lime and pyroclastic rock through macroscopic observations of the present concrete fabric and ancient texts. This information is used to compute the thermal history of the 10 m^2 by 5.7 m thick *pilae*, where adiabatic time-temperature profiles are calculated from an estimation of heat evolved during formation of C-A-S-H to identify the maximum temperature at which Al-tobermorite crystallized. Finally, the lime-seawater-volcanic ash mix design and massive scale of the Roman seawater concrete constructions are discussed as determining factors in generating temperatures sufficient for large-scale synthesis of the crystals. These observations advance an ancient concept of concrete produced with lime and pyroclastic rock, which opens future perspectives for producing Al-tobermorite in the context of highly durable concrete structures with volcanic pozzolans.

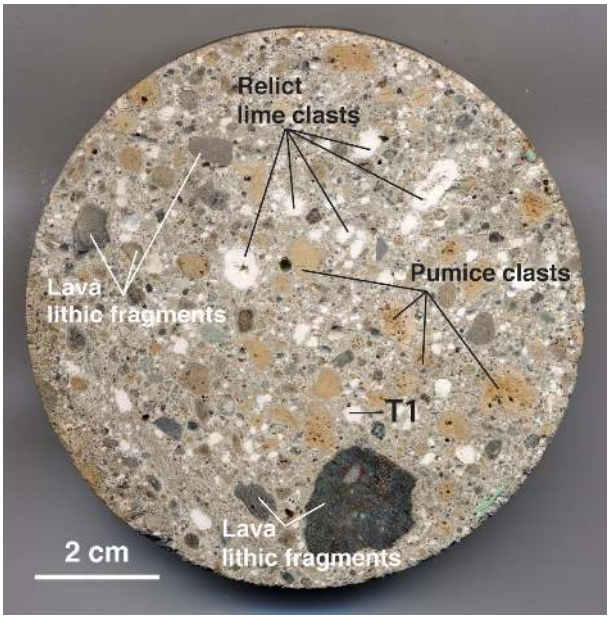

FIGURE 2. Hydrated lime-volcanic ash mortar of the concrete drill core. The volcanic ash pozzolan (*pulvis*) is composed of yellowish gray (5Y/2) pumice clasts, dark gray (N2) lava lithic fragments, and sanidine and clinopyroxene crystals. STXM and NMR analyses used the T1 Al-tobermorite specimen.

EXPERIMENTAL METHODS

Materials

The *Baianus Sinus* concrete breakwater was cored by the ROMACONS drilling program in 2006 (BAI.06.03) (Fig. 1); the *Portus Neronis* concrete was cored in 2002 (ANZ.02.01) in collaboration with CTG Italcementi Laboratories in Bergamo, Italy (Oleson et al. 2004; Brandon et al. 2008). At the time of investigation, the concrete had been exhumed from the original structure submerged in seawater and exposed to the subaerial environment for ~6 to 10 years in plastic core boxes in Bergamo. The core was sliced into 1 cm thick disks in 2011, and the concrete fabric remains fresh and intact on these surfaces. All sawing was performed with kerosene. Thin section blocks were impregnated with epoxy, and kerosene was used in grinding and polishing; no water was employed in the preparations of the sections. The STXM and NMR studies used the lime clast labeled T1 in Figure 2. Whole pumice clasts were delicately pried and scraped from the mortar using a Leitz stereomicroscope, to obtain all glass and crystals and remove adhering binder.

Scanning electron microscopy

Major element compositions of another *Baianus Sinus* relict lime clast (Figs. 3a and 3b) were acquired with an EDAX TSL energy-dispersive X-ray spectrometer on the Zeiss EVOMA10 scanning electron microscope at the Department of Earth and Planetary Science at UC Berkeley. Operating conditions were beam energy of 15 keV, beam current of 850 pA, and counting time of 10 s with 3500 counts per second. Counts were then converted to semiquantitative concentrations and atomic ratios for Ca, Si, and Al. The linescan compositions (Fig. 3c), measured at 0.5 µm spacing, were averaged over 5 data points.

X-ray powder diffraction analyses (XRPD)

X-ray diffraction of an Al-tobermorite specimen from another lime clast (Fig. 4) was performed at beamline 12.2.2 of the Advanced Light Source at the Lawrence Berkeley National Laboratory (Kunz et al. 2005) using a synchrotron monochromatic X-ray beam with a 0.6199 Å (20 keV wavelength) under ambient conditions. The finely ground specimen was exposed to X-rays at a 238 mm sample-to-detector distance for 300 s.

The BAI.06.03P1 and BAI.03.01P1 pumice specimens were finely ground dry in an agate mortar and standard XRPD analyses were performed with a Bruker D8-advance X-ray diffractometer at CTG Italcementi Laboratories in Bergamo, Italy, equipped with Cu$K\alpha$ radiation, two sets of Soller slits (2.5° aperture) and a LynxEye PsD Detector on a Si-stray holder and front loading. XRPD spectra were collected from 5 to 70° 2θ with a step size = 0.02°, 0.4 s per step, D.S. = 0.5°, R.S. = 8 mm, Ni-filter, spinner rotation = 30 rpm, generator voltage 40 kV, and current 40 mA, using the DIFFRAC Plus EVA ver.15.0.0.0 (Bruker-AXS) data processing software and the applicable ICDD card file numbers (PDF-2 Database, Volume Release 2001, data sets 1–51 and 70–89).

Trace element analysis

Major and trace element compositions were determined from 3 to 4 g of powdered grayish orange 10YR 7/4 to 10YR 8/4 and light medium gray (N6) pumice clasts (Geological Society of America Rock-Color Chart 1995), 0.75 to 1.5 cm diameter, and fragments of grayish orange 10YR 7/4 pumiceous tuff using lithium metaborate/tetraborate fusion ICP whole rock for major elements and ICP/MS for trace elements at Activation Laboratories in Ancaster, Ontario, Canada (Fig. 5; Table 1), which blends HT-digestion in excess Li-borate (typical for whole-rock XRF) with dissolution in strong acid to prepare for ICP-AES analysis. The lowermost trace element detection limit in the Code4B2 research package is 0.5 ppm for Y, 1 ppm for Zr, 0.2 ppm for Nb, and 0.1 ppm for La, and 0.01 for Yb, as for the tuff specimens; however, the Code4B2 standard analyses of the pumice specimens have lower resolutions, listed in Table 1. See Supplemental Table 2[1] for the complete analyses.

[1] Deposit item AM-13-1003, Supplemental Tables 1 and 2. Deposit items are available two ways: For a paper copy contact the Business Office of the Mineralogical Society of America (see inside front cover of recent issue) for price information. For an electronic copy visit the MSA web site at http://www.minsocam.org, go to the *American Mineralogist* Contents, find the table of contents for the specific volume/issue wanted, and then click on the deposit link there.

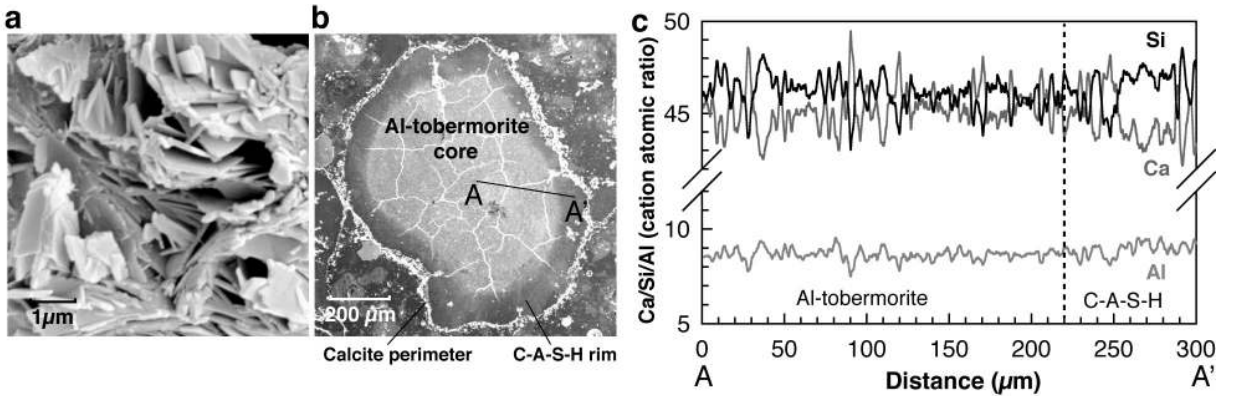

FIGURE 3. Relict lime clast microstructures. (**a**) SEM secondary electron image of Al-tobermorite plates, (**b**) SEM backscatter electron image of a completely transformed lime clast. Bright spots along the perimeter are calcite. Note the gradual transition from the C-A-S-H rim to Al-tobermorite in the interior, indicated by the dotted line in panel **c**, showing normalized atomic ratios (Ca+Al+Si = 100) along profile A-A′, by SEM-EDS.

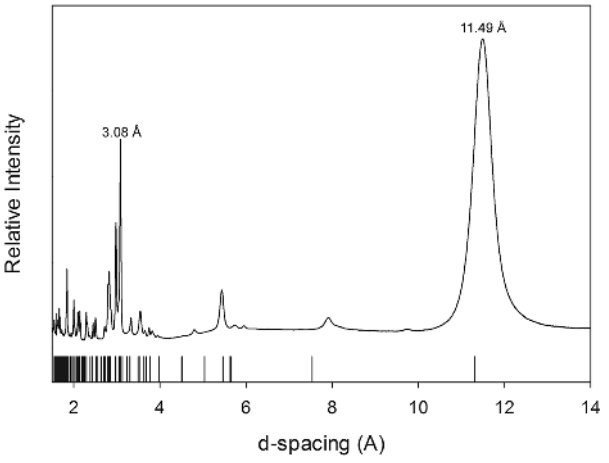

FIGURE 4. Powder X-ray diffraction pattern of *Baianus Sinus* Al-tobermorite from a synchroton radiation experiment under ambient conditions. The vertical lines on the x-axis are diffraction peaks diffraction peaks of 11Å tobermorite from Merlino et al. (2001).

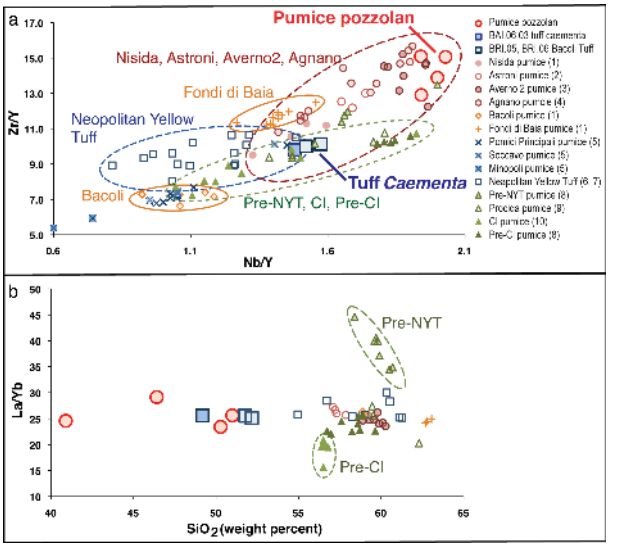

FIGURE 5. Provenance of pyroclastic rock in the ancient Pozzuoli Bay concretes (Table 1). Volcanic chronostratigraphy of post-Neapolitan Yellow Tuff (NYT) Flegrean Fields eruptive deposits from $^{40}Ar/^{39}Ar$ dating by Fedele et al. (2011). Numbered references are: Epoch III (red): 1 = Nisida pumice, Fedele et al. (2011); 2 = Astroni pumice, Tonarini et al. (2009); 3 = Averno 2 pumice, Di Vito et al. (2011); 4 = Agnano pumice, de Vita et al. (1999). Epoch II (orange): 1 = Bacoli pumice, Fedele et al. (2011); 1 = Fondi di Baia pumice, Fedele et al. (2011). Epoch I (blue): 5 = Pomici Principali pumice, Soccavo pumice, Minopoli pumice, Lustrino et al. (2002); 6 and 7 = Neapolitan Yellow Tuff, Orsi et al. (1992), Scarpati et al. (1993). Pre-Neapolitan Yellow Tuff deposits (green): 8 = Pre-Neapolitan Yellow Tuff pumice, Pabst et al. (2008); 9 = Procida pumice, De Astis et al. (2004); 10 = Campanian Ignimbrite pumice, Civetta et al. (1991); 8 = Pre-Campanian Ignimbrite pumice, Pabst et al. (2008).

STXM experiments

Scanning transmission X-ray microscopy (STXM) analyses were performed at the Advanced Light Source at the Lawrence Berkeley National Laboratory (Kilcoyne et al. 2003) (Figs. 6 and 7). Near-edge X-ray absorption fine structure (NEXAFS) spectra were obtained for C *K* and Ca L_2,L_3 edges at beamline 5.3.2.2, and for Al *K* and Si *K* edges at beamline 5.3.2.1. The T1 Al-tobermorite specimen was extracted from a relict lime clast (Fig. 2), powdered using mortar and pestle, diluted in ethanol, and deposited onto a 100 nm thick SiN_3 window with a micropipette (Fig. 7a). Another relict hydrated lime clast was cut from a removable polished thin section, placed on a copper grid, and ion-milled (Fig. 6a).

STXM data acquisition operates inside a high-vacuum chamber flushed with He gas (McKeown et al. 1985; Kilcoyne et al. 2010; Prince et al. 1999). Calibration at beamline 5.3.2.2 was performed by adjusting the monochromator settings until the characteristic Rydberg state excitation peaks of CO_2 gas at the C-*K* edge matched known values; calibration for beamline 5.3.2.1 was performed in a similar fashion by setting the absorption edge inflection point of aluminum foil and pure silicon at 1559.3 and 1838.9 eV, respectively. Image stacks were obtained by scanning the sample area at each point of the pre-defined energy ranges, ranging from 0.1 to 2 eV increments, depending on expected feature sharpness. Each point on a NEXAFS spectrum (Figs. 6d, 6e, and 7b) represents an averaged normalized optical density at a specific energy value of all pixels contained in a selected area. Brightness, or optical density, is a function of composition, density, and sample thickness. It is calculated at each pixel as a linear log of the ratio between the averaged transmitted intensity of the sample-free region and transmitted photon intensity. The element maps (Figs. 6b, 7d, and 7e) are obtained by computing the optical density for all pixels between the energies immediately before and close to a characteristic absorption peak. Axis 2000 software was used to align image stacks, to compute element maps, and to extract NEXAFS spectra (Hitchcock 2011).

NMR study

The ^{29}Si and ^{27}Al NMR studies (Figs. 8a and 8b) were performed at the Advanced Nanofabrication Imaging and Characterization Laboratories, King Abdullah

TABLE 1. Whole rock compositions of pumice clasts in Bay of Pozzuoli seawater concretes (BAI.06.03P), in *Baianus Sinus* tuff coarse aggregate (BAI.06.03T), and Bacoli Tuff (BRI.T) in weight percent (wt%) of main element oxides, by ICP-AES

		Baianus Sinus (BAI.06)				Bacoli Tuff (BRI)			XRF data		
	LLD	.03P1	.03P2	.01P1	.05.P2	.03.T1	.05.T1	.06.T1	Bacoli Tuff†	Pozzolan ‡	Pozzolan §
		pumice (mortar)	pumice (mortar)	pumice (mortar)	pumice (mortar)	tuff (caementa)	tuff (caementa)	tuff (caementa)	Flegrean pyroclastic deposits		
Major element compositions (wt%)											
SiO_2	0.01	40.90	50.28	46.41	50.99	49.18	51.77	52.17	52.45	53.08	57.08
Al_2O_3	0.01	14.48	14.83	15.46	15.91	14.90	15.33	15.33	15.45	17.89	18.34
Fe_2O_3(T)	0.01	2.53	3.06	2.58	3.00	3.47	3.49	3.47	3.42	4.29	2.2
MnO	0.001	0.104	0.141	0.116	0.132	0.107	0.110	0.110	n.d	n.d	n.d
MgO	0.01	0.48	4.62	0.51	4.81	3.63	0.85	0.80	0.83	1.23	0.97
CaO	0.01	11.49	2.63	7.55	1.89	1.79	2.48	2.41	2.37	9.05	3.15
Na_2O	0.05	3.60	4.31	4.40	4.43	4.33	3.65	3.04	3.33	3.08	4.18
K_2O	0.01	5.01	5.34	6.93	5.92	5.81	7.75	7.87	7.85	7.61	8.05
TiO_2	0.001	0.305	0.382	0.338	0.405	0.391	0.381	0.385	n.d	n.d	n.d
P_2O_5	0.01	0.06	0.08	0.05	0.07	0.13	0.13	0.13	n.d	n.d	n.d
LOI*	0.01	20.99	15.28	16.23	13.38	16.73	14.12	14.14	13.41	3.05	3.75
Sum	–	99.95	101.00	100.60	100.90	100.50	100.10	99.86	99.11	99.28	97.72
Trace element contents (ppm)											
Y	2; 0.5	27	33	34	34	25.7	24.2	25.9			
Zr	4; 1	375	498	439	512	252	245	259			
Nb	1; 0.2	54	64	66	69	38	38.1	39.4			
La	0.5; 0.1	73.7	79.6	99.1	87.1	60.9	58.8	63.3			
Yb	0.1; 0.01	3.0	3.4	3.4	3.4	2.38	2.30	2.52			
Trace element ratios‖											
Zr/Y		14	15	13	15	10	10	10			
Nb/Y		2	2	2	2	1	2	2			
La/Yb		25	23	29	26	26	26	25			

Notes: Trace elements from the same samples in parts per million (ppm), by ICP-MS, and calculated trace element ratios. Flegrean pyroclastic deposits whole rock compositions by XRF. Further explananation in text.
* Determined gravimetrically.
† Bacoli quarry, also BRI.05.T1, BRI.06.T used in the Brindisi concrete reproduction (Oleson et al. 2006).
‡ Bacoli pozzolan analysis (1) in Costa and Massazza (1974, p. 6), also quoted as analysis (1) in Massazza (2004, p. 475).
§ Bacoli pozzolan analysis (1) from Sersale and Orsini (1969, p. 114).
‖ See Supplemental Table 2 for complete trace element analyses.

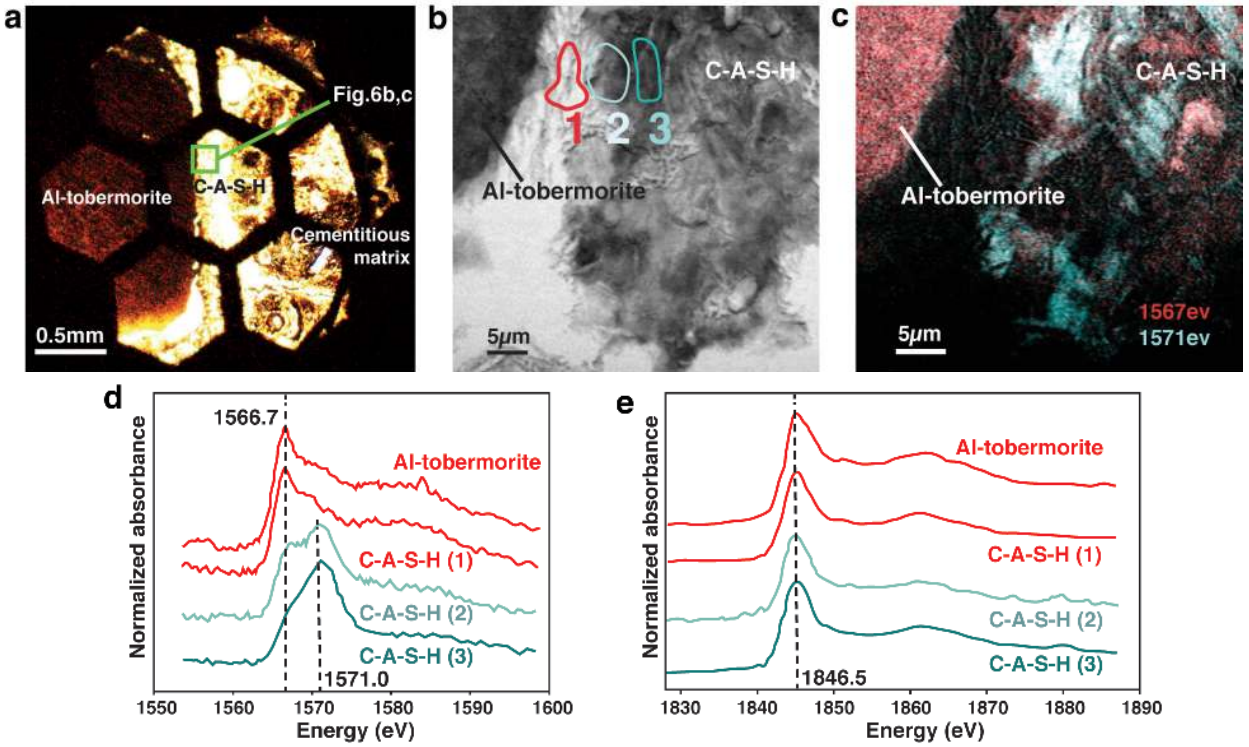

FIGURE 6. Bonding environments of Al^{3+} and Si^{4+} in *Baianus Sinus* Al-tobermorite and C-A-S-H. (**a**) Optical image of relict lime clast in sample holder prior to ion-milling, showing crystalline Al-tobermorite core, complex C-A-S-H perimetral rim, and pumiceous cementitious matrix. (**b**) STXM absorption contrast image at 1550 eV Al-edge; lighter areas generally correspond to less absorption because less material is present. (**c**) STXM map of $Al^{[IV]}$ at 1567 eV (red), $Al^{[VI]}$ at 1571 eV (cyan), and mixed $Al^{[IV]}$ and $Al^{[VI]}$ (white). (**d**) Typical aluminum *K*-edge, (**e**) silicon *K*-edge NEXAFS spectra for Al-tobermorite and C-A-S-H, showing typical spectra at sites (1), (2), and (3) of part **b**.

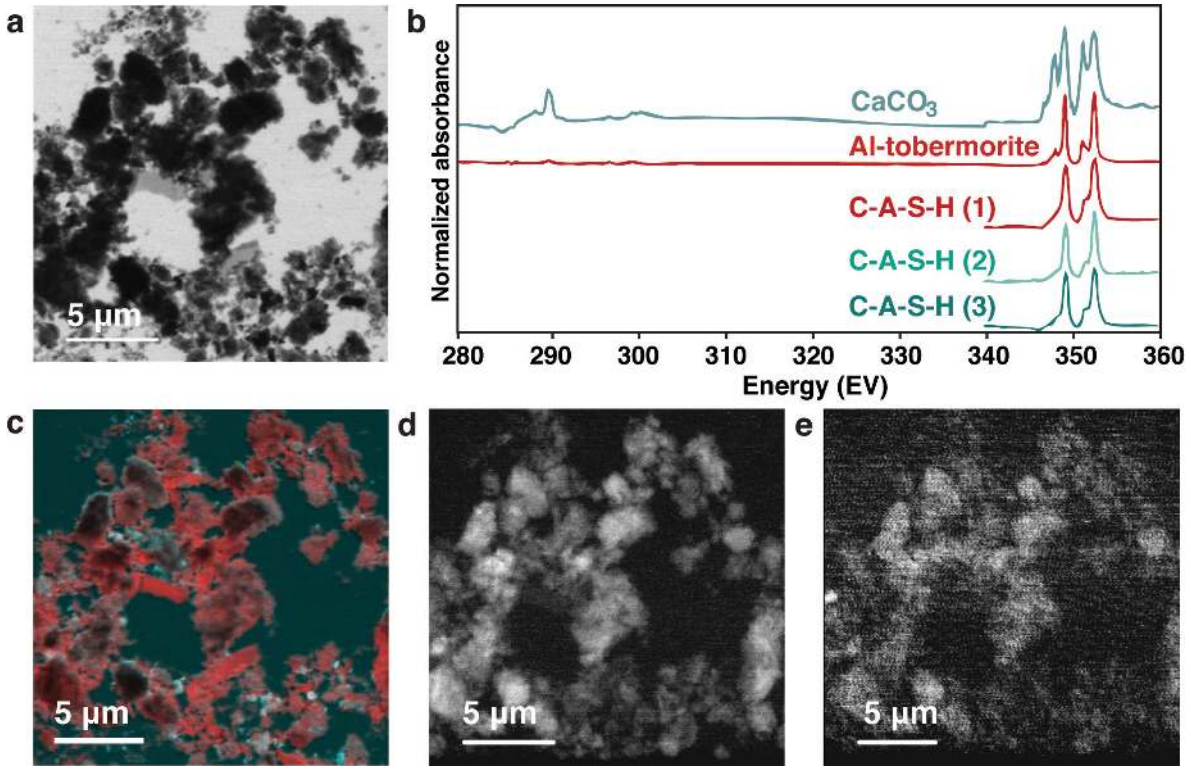

Figure 7. Scanning transmission X-ray microscopy (STXM) images. Powdered *Baianus Sinus* Al-tobermorite T1 specimen (**a**–**e**) and ion-milled C-A-S-H specimen (**b**). (**a**) Simple absorption contrast image of the Al-tobermorite phase at 290.3 eV. (**b**) Typical carbon *K*-edge and calcium L_3,L_2 edge NEXAFS spectra peaks for the uncarbonated Al-tobermorite phase, small inclusions of $CaCO_3$, and the C-A-S-H phase. (**c**) Carbon and calcium composite map of part **a**, showing Al-tobermorite particles; red regions contain only calcium and cyan regions contain both carbon and calcium. (**d**) Silicon map (1838/1846.5 eV) and (**e**) aluminum map (1560/1566 eV) of part **a**. Brightness reflects optical density values in all maps (see text).

University of Science and Technology, Saudi Arabia, with 50 mg of the finely ground T1 specimen packed into a 4 mm zirconia rotor and sealed at the open end with a Vespel cap. The rotor was spun at 14 kHz on a Bruker Ultrashield 400WB Plus with a 9.4 T magnet, operating at 104.26 MHz for ^{27}Al and 79.495 MHz for ^{29}Si. The magic angle in both cases was set using KBr to 54.734°.

Electron microprobe analysis

Major element compositions of clusters of 3 to 5 µm long Al-tobermorite crystals (Fig. 9; Table 2) were acquired in the UC Berkeley Electron Microprobe Laboratory in the Department of Earth and Planetary Science from polished thin sections of mortars prepared according to the hydrophobic specifications described above for the SEM-EDS specimen, but with different relict lime clasts. The Cameca SX-51 electron microprobe is equipped with five tunable wavelength-dispersive spectrometers. The samples were analyzed using a 40° takeoff angle, 15 keV beam energy, 10 nA beam current, and a 1 µm beam diameter. A 10 s counting time on peak and background was used for all elements and the analyses were corrected using ZAF matrix corrections. To account for potential Na and K loss and/or Si and Al gain, these elements were set to be analyzed first in each analysis (Morgan and London 2005). In addition, a time-dependent intensity calibration was applied to Na, K, Al, and Si using the software Probe for EPMA (v. 8.69). Oxygen and water content were calculated by stoichiometry. The fine grain size of Al-tobermorite in thin section contributed to lower wt% oxide measurements. Analyses with unreasonably low-wt% oxide totals (with H_2O calculated by stoichiometry) and low atoms per formula unit were omitted from Table 2. Supplemental Table 1 reports tobermorite compositions from microprobe analyses in the geologic literature.

Modeling of time-temperature profiles

The adiabatic temperature-time profiles of the *Baianus Sinus* breakwater (Fig. 10) use finite element analysis implementing the Structural Analysis Program for Temperature and Stress (SAPTS) program developed at Tsinghua University, China, designed to compute the evolution of temperatures associated with heats of hydration of cementitious components in large concrete dams (Zhu 1999; Li 2007), with reasonable boundary conditions. Thermal properties of the Neapolitan Yellow Tuff and the heat evolution profile come from previous literature (Appendix 1). The approximate maximum adiabatic temperature is $\Theta = m_c Q_1 / C\rho$, where Θ is the adiabatic temperature, m_c is the unit weight of cementitious hydrates in the concrete, Q_1 is the evolution of heat of hydration from the C-A-S-H cementitious component, C is the specific heat capacity of the whole concrete, and ρ is the unit weight of the BAI.06.03 drill core concrete.

Results

Relict lime clast microstructures

Dense clusters of platey Al-tobermorite crystals (Fig. 3a) occur in the centers of partially dissolved relict lime clasts (Fig. 3b). The crystals are surrounded by perimetral zone of C-A-S-H that is optically isotropic in cross-polarized light, but does contain occasional sparry calcite. A rim of calcite <30 µm wide surrounds the lime relict. A compositional traverse across the relict lime clast shows that cation atomic ratios, as Ca, Si, and Al divided by Ca+Si+Al = 100, remain in well-defined ranges in both the Al-tobermorite and C-A-S-H zones (Fig. 3c). The average composition of each zone is Ca/(Si+Al) ~ 0.79. These values are typical of other relict lime microstructures, but the relative proportion of C-A-S-H to Al-tobermorite varies with clast size; smaller particles are almost wholly dissolved. The X-ray diffraction pattern of the Al-tobermorite shows high purity and a distinct interlayer spacing of 11.49 Å (Fig. 4, see also Jackson et al. 2013).

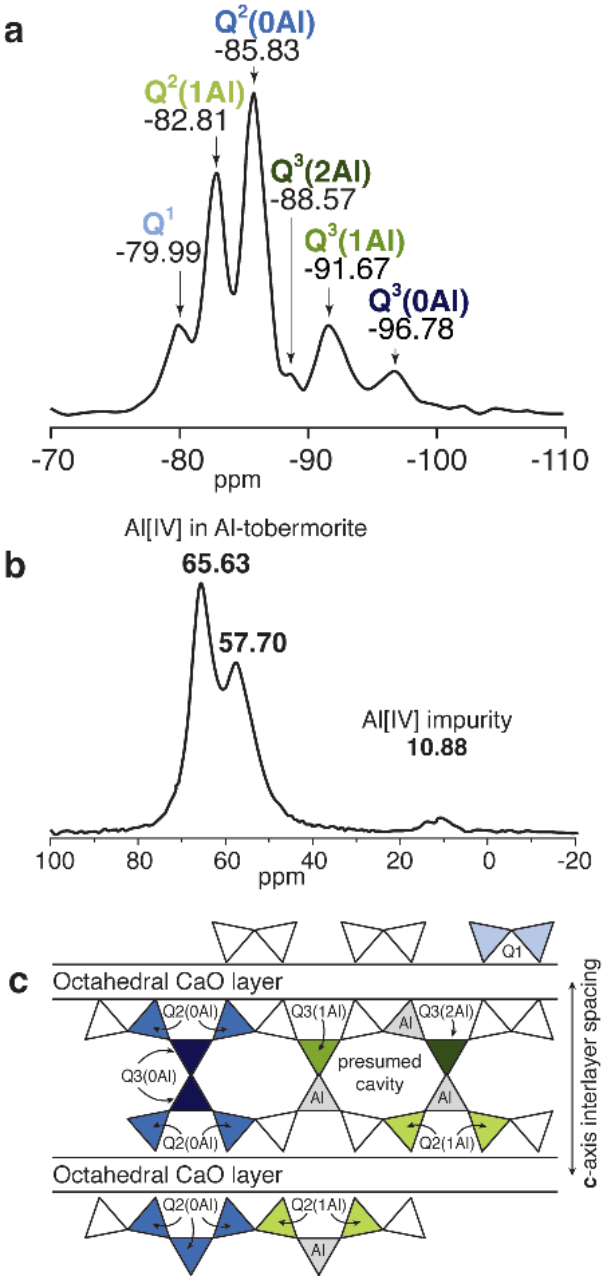

FIGURE 8. Results of NMR analysis of the T1 Al-tobermorite specimen. (**a**) ^{29}Si NMR study; Q^1 dimers or chain terminations, Q^2 chain middle groups, and Q^3 branching sites describe the connectivity of SiO_2 tetrahedra. (**b**) ^{27}Al NMR study. (**c**) Schematic diagram showing types of measured linkages of tetrahedral SiO_4^{4-} or AlO_4^{5-} units (triangles). Blue triangles indicate examples of linkages of silicate tetrahedra and green triangles indicate linkages of silicate and aluminum tetrahedra.

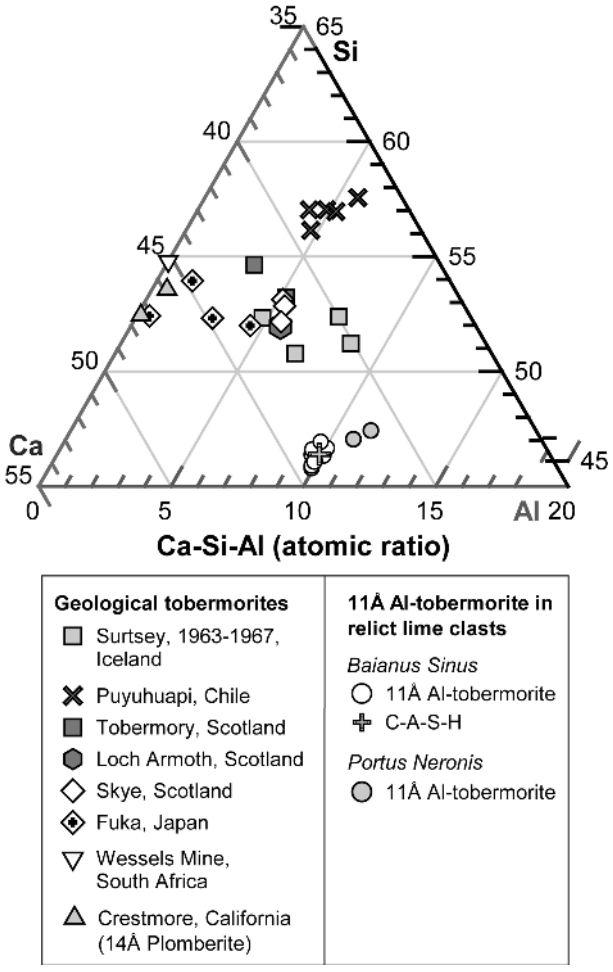

FIGURE 9. Compositions of geological and archaeological tobermorites. Al-tobermorite from hydrothermal environments in volcanic rocks and tobermorite from calc-silicate rocks reported in the geologic literature, the *Baianus Sinus* and *Portus Neronis* Al-tobermorite, and *Baianus Sinus* C-A-S-H. Ca/Si/Al = 100 as atomic ratios from microprobe analyses of the tobermorites and SEM-EDS analyses of *Baianus Sinus* C-A-S-H (Table 2 and Supplemental Table 2).

C-A-S-H and Al-tobermorite NEXAFS spectra and aluminum coordination

Figures 6, 7, and 8 illustrate Al^{3+} and Si^{4+} bonding environments in *Baianus Sinus* Al-tobermorite and C-A-S-H. STXM mapping determines the nanoscale (<25 nm) distribution of chemical species and their local bonding environments. In addition to two-dimensional absorption contrast images (Figs. 6b, 7d, and 7e) the energy stack image produces a NEXAFS spectrum for a specific element on each pixel of the image (Figs. 6d, 6e, and 7b). ^{29}Si NMR describes the connectivity of silicate tetrahedron via oxygen on a scale of the relative abundance of $Q^n(m\text{Al})$, where Q^n silicate tetrahedra are connected via n bridging O atoms to m Al^{3+} (Fig. 8a). For a typical relict lime clast microstructure (Fig. 6a), the STXM absorption contrast image at 1550 eV (Fig. 6b) shows Al^{3+} compositional abundance. The spectroscopic map (Fig. 6c) shows Al^{3+} coordination with oxygen through this area, where red shows tetrahedral coordination (^{IV}Al) at 1567 eV and cyan shows octahedral coordination (^{VI}Al) at 1571 eV (Li et al. 1995; Kato et al. 2001). Al-tobermorite has homogeneous Al *K* absorption at 1567 eV, but C-A-S-H has heterogeneous absorption environments.

C-A-S-H. Although C-A-S-H in the perimetral rim of the partially dissolved relict lime clast has a constant ^{IV}Si absorption peak at 1846.5 eV {Fig. 6e [C-A-S-H spectra (1), (2), (3)]} some

Table 2. Mineral compositions of Al-tobermorite in relic lime clasts A–E from *Baianus Sinus* and *Portus Neronis*, in weight percent (wt%) of oxides, by EPMA (Fe_2O_3 represents "total iron")

Oxide	3σ LLD*	*Baianus Sinus* (Bay of Pozzuoli)																		*Portus Neronis* (Anzio)				Tobermorite	
		BAI.06.03 A						BAI.06.03 B				BAI.06.03 C				BAI.06.03 D				ANZ.02.01 E				Skye†	Ideal‡
			±2σ§		±2σ		±2σ		±2σ		±2σ		±2σ		±2σ		±2σ		±2σ		±2σ		±2σ		
SiO_2	0.04	38.7	0.5	39.7	0.5	39.0	0.5	39.5	0.5	39.1	0.5	38.6	0.5	38.6	0.5	39.0	0.5	40.6	0.5	39.4	0.5	39.9	0.5	48.1	48.2
Al_2O_3	0.04	7.1	0.2	7.0	0.2	7.1	0.2	7.3	0.2	7.1	0.2	6.7	0.2	7.0	0.2	7.1	0.2	7.1	0.2	7.7	0.2	8.1	0.2	4.0	0.0
Fe_2O_3	0.13	<0.13	0.0	<0.13	0.0	<0.13	0.0	<0.13	0.0	<0.13	0.0	<0.13	0.0	<0.13	0.0	0.2	0.2	<0.13	0.0	<0.13	0.0	0.2	0.0	0.0	0.0
MgO	0.02	0.2	0.1	0.2	0.1	0.1	0.0	0.4	0.1	0.2	0.1	0.7	0.1	0.2	0.1	0.1	0.0	0.0	0.0	1.8	0.1	1.7	0.1	0.0	0.0
CaO	0.03	35.0	0.5	35.2	0.5	35.1	0.5	34.7	0.5	34.9	0.5	33.9	0.5	34.5	0.5	33.8	0.5	35.0	0.5	32.9	0.5	32.4	0.5	35.2	37.4
Na_2O	0.05	0.7	0.1	0.6	0.1	1.2	0.2	1.5	0.2	1.6	0.2	0.7	0.1	1.4	0.2	2.2	0.2	1.9	0.2	1.7	0.2	2.5	0.2	0.0	0.0
K_2O	0.03	1.0	0.1	1.0	0.1	1.0	0.1	1.2	0.1	1.2	0.1	0.9	0.1	1.0	0.1	0.9	0.1	0.8	0.1	0.7	0.1	0.9	0.1	0.0	0.0
Sum		82.7	0.7	83.6	0.7	83.4	0.8	84.4	0.8	84.1	0.8	81.6	0.7	82.8	0.8	83.3	0.8	85.4	0.8	84.2	0.8	85.8	0.8	87.3	85.6
H_2O||		11.0		11.3		11.3		11.4		11.3		11.0		11.0		11.1		11.6		11.7		12.0		12.5	14.4
																									100
Number of atoms per formula unit based on 18[O, (OH)]																									
Si		4.8	0.04	4.9	0.03	4.8	0.04	4.8	0.04	4.8	0.04	4.8	0.04	4.8	0.04	4.8	0.04	4.9	0.03	4.8	0.04	4.7	0.04	5.5	6.00
Al		1.0	0.03	1.0	0.03	1.0	0.03	1.0	0.03	1.0	0.03	1.0	0.03	1.0	0.03	1.0	0.03	1.0	0.03	1.1	0.03	1.1	0.03	0.5	0.00
Fe^{3+}		0.0	0.00	0.0	0.00	0.0	0.00	0.0	0.00	0.0	0.00	0.0	0.00	0.0	0.00	0.0	0.02	0.0	0.00	0.0	0.00	0.0	0.00	0.0	0.00
Mg		0.0	0.01	0.0	0.01	0.0	0.01	0.1	0.01	0.0	0.01	0.1	0.02	0.0	0.01	0.0	0.01	0.0	0.01	0.3	0.02	0.3	0.02	0.0	0.00
Ca		4.6	0.06	4.6	0.06	4.6	0.06	4.5	0.06	4.6	0.06	4.6	0.06	4.6	0.06	4.5	0.06	4.5	0.06	4.3	0.06	4.1	0.06	4.3	5.00
Na		0.2	0.03	0.1	0.03	0.3	0.04	0.3	0.04	0.4	0.04	0.2	0.03	0.3	0.04	0.5	0.05	0.4	0.04	0.4	0.04	0.6	0.05	0.0	0.00
K		0.2	0.01	0.2	0.01	0.2	0.01	0.2	0.02	0.2	0.02	0.1	0.01	0.2	0.01	0.1	0.01	0.1	0.01	0.1	0.01	0.1	0.01	0.0	0.00
Sum		10.8	0.08	10.8	0.08	10.9	0.09	10.9	0.09	11.0	0.09	10.8	0.09	10.9	0.09	11.0	0.09	10.9	0.09	10.9	0.09	11.0	0.09	10.3	11.00
Ca/(Al+Si)		0.80		0.79		0.79		0.77		0.79		0.78		0.79		0.76		0.77		0.73	0.70		0.68		0.78
Al/(Al+Si)		0.18		0.17		0.18		0.18		0.18		0.17		0.18		0.18		0.17		0.19	0.19		0.08		0.00

* Lower limit of detection.
† Analysis 8 in Livingstone (1988, p. 712), also quoted as analysis 2 in Anthony et al. (1995, p. 808).
‡ Ideal tobermorite of stoichiometric composition without impurities.
§ Calculated by propagating the analytical uncertainty following Giarimita and Day (1990).
|| Calculated by stoichiometry.

nanoscale areas have a prominent 1566.7 peak {Figs. 6c and 6d {C-A-S-H spectrum (1)]} indicating predominantly ^{IV}Al. This may correspond to an ancient analog of tobermorite-like C-A-S-H (Sun et al. 2006; Lothenbach et al. 2011), or it could be a mixture with Al-tobermorite, which occurs in the center of the lime clast. In some areas, a 1571.0 eV peak indicating ^{IV}Al in octahedral coordination predominates {Figs. 6c and 6d [C-A-S-H spectrum (3)]} while in other areas tetrahedral ^{IV}Al at 1566.7 and ^{VI}Al at 1571 occur together {Figs. 6c and 6d [C-A-S-H spectrum (2)]} In experimental syntheses of C-A-S-H with low Ca/(Si+Al) = 0.86, ^{V}Al and ^{VI}Al may increase with hydration time. These occur in hydrous aluminate, Ca-aluminate, or Na-aluminate environments in interlayer cavities and on octahedral layer surface environments (Sun et al. 2006; Sasaki et al. 1996).

Al-tobermorite. Absorption contrast element maps of the powdered T1 specimen (Figs. 7d and 7e) indicate that presence of aluminum correlates with silicon in most areas, suggesting that Al^{3+} substitution is omnipresent at nanoscale resolution (<25 nm). The Al-tobermorite clusters are not entirely homogeneous, however. A sharp peak on the carbon (C) edge spectra at 290.3 eV coupled with calcium L_3 and L_2 double peaks (Fig. 7b), where the ratio between the 349.2 and 348.0 eV peak height and 352.5 and 351.2 eV peak heights are about 1:1, indicate that small amounts of calcite ($CaCO_3$) are present (Benzerara et al. 2004). The characteristic NEXAFS spectra for the powdered Al-tobermorite (Figs. 6d and 6e) show single Al^{3+} and Si^{4+} absorption peaks at 1566.7 and 1846.5 eV, respectively, indicating tetrahedral coordination for either element (Li et al. 1995; Kato et al. 2001). Asymmetric broadening of the Al^{3+} peak at 1566.6 to 1568.0 eV, however, indicates distortions in Al-O bond distances and AlO_4 tetrahedra, suggesting diverse environments of Al^{3+} substitution for Si^{4+}.

The ^{29}Si NMR analysis (Fig. 8a) indicates that the alumina tetrahedra occur in silicate chain [Q^2(1Al)] and branching [Q^3(1Al), Q^3(2Al)] positions within the (002) interlayer (Komarneni and Roy 1983; Komarneni et al. 1985; Tsuji et al. 1991; Skibsted et al. 1994; Sun et al. 2006). The high intensity of Q^2(0Al) and Q^2(1Al) peaks relative to the Q^1 peak indicates long chain lengths in the **b** [020] crystallographic direction. The ^{29}Si NMR results are further clarified with ^{27}Al NMR peaks in the tetrahedral range of 50–80 ppm (Fig. 8b), which confirm two different environments for ^{IV}Al: Q^2(1Al) bridging sites at 65.63 ppm and Q^3(1Al) branching sites at 57.70 ppm (Sun et al. 2006; Houston et al. 2009; Tsuji et al. 1991; Komarneni et al. 1985). The Q^3(2Al) substitution is apparently not present in sufficient quantities to be resolved on the ^{27}Al spectra.

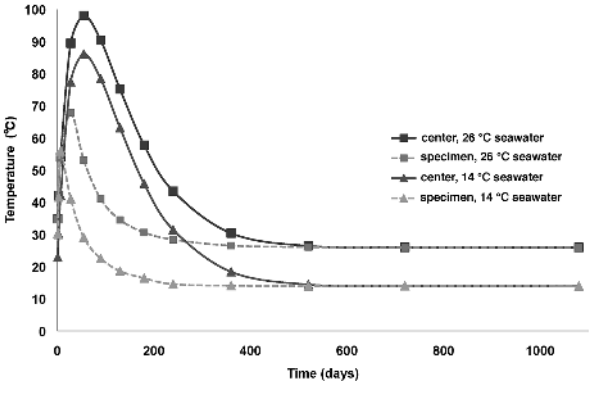

Figure 10. Maximum temperatures (Q) at the specimen site and the body center of the 5.7 m thick *Baianus Sinus* block. The model configuration (Appendix 1) calculates heat evolved through formation of C-A-S-H cementitious binder. Exothermic hydration of lime produced an initial temperature of about +5 °C above ambient seawater temperatures (T_w). The model block attained 14–26 °C seawater temperatures about two years after installation (Appendix Table 2).

The higher intensity of the 65.63 peak relative to 57.70 indicates that there is more aluminum in the bridging Q^2(1Al) sites of the silicate chains than the branching sites Q^3(1Al). A schematic diagram (Fig. 8c) illustrates these bonding environments.

Pyroclastic rock trace element analysis

For seawater mortar, Vitruvius and Pliny the Elder stated a preference for powdery ash (*pulvis*) "quarried from the region that runs from Cumae to the promontory of Minerva" and, more specifically, "in the vicinity of Baiae and the territory of the municipalities around Mount Vesuvius" and "the hills of Puteoli" (Fig. 2; Appendix 1). Archaeologists have hypothesized that Romans shipped tens of thousands of tons of Flegrean pyroclastic rock to ports throughout the Mediterranean (Oleson et al. 2004), but the provenance of the pyroclastic rock that occurs in the Bay of Pozzuoli structures (Fig. 1) as discrete ash- to lapilli-sized particles in the mortar and as decimeter-sized tuff coarse aggregate has not been precisely identified. Although the pumice altered during pozzolanic reaction, ratios of immobile, incompatible trace elements should provide indications of lithologic provenance when compared with published analyses of powdered geologic specimens (Lustrino et al. 2002). In particular, zirconium/yttrium (Zr/Y) and niobium/yttrium (Nb/Y) ratios have been shown to be accurate indicators of eruptive provenance in the central Italian volcanic districts (Marra et al. 2011). Over the past 30 ka, numerous eruptions within the Flegrean Fields volcanic district have produced pumice deposits in the area described by Vitruvius and Pliny. Figure 5 shows the complex distribution of the trace element compositions of these pumices, even within a specific eruptive unit, using the Epoch I, II, and III eruptive chronstratigraphy of Fedele et al. (2011).

Tuff coarse aggregate. Specimen BAI.06.03T1 is a fragment of the compact grayish yellow (10YR 7/4) vitric-crystal tuff coarse aggregate (*caementa*, as described below) of the *Baianus Sinus* concrete, with primary illite, sanidine, and authigenic analcite, phillipsite, chabazite, and calcite. It is similar to grayish yellow (10YR 7/4) pumiceous tuff quarried at Bacoli, with primary sanidine, and authigenic analcite, phillipsite and chabazite, for the 2004 experimental reproduction of Roman maritime concrete at Brindisi (Oleson et al. 2006; Vola et al. 2011a): 05.BRI.02.T1 and 06.BRI.C1.T1 are coarse aggregate of that experimental 2 m^3 concrete block, drilled one and two years after installation. The *Baianus Sinus* and Bacoli whole rock tuff specimens have similar Zr/Y and Nb/Y values, 9.81 to 10.12 and 1.48 to 1.57, respectively, suggesting a common Bacoli source; Zr/Y coincides with the whole rock NYT analyses, but Nb/Y falls in the high end of the compositional field (Table 1; Fig. 5a) (Orsi et al. 1992; Scarpati et al. 1993). Lanthium and ytterbium (La/Yb) ratios also coincide with those of the NYT (Fig. 5b). The voluminous NYT erupted at about 15 ka, and the Bacoli Tuff erupted at about 8.6 ka; it forms ash ring deposits near Baia (Fig. 2b) (Fedele et al. 2011).

Pumice pozzolan. *Bainus Sinus* specimen BAI.06.03P1 and *Portus Baianus* specimen BAI.06.01P1 are composed of grayish orange (10YR 8/4) pumices with primary illite, sanidine, and anorthite, and authigenic phillipsite, calcite, and Al-tobermorite. *Baianus Sinus* specimen BAI.06.03P3 and *Portus Iulius* specimen BAI.06.05P2 are composed of light medium (N6) gray glassy pumices with a similar primary crystal assemblage, determined petrographically, but with no Al-tobermorite. All four specimens have similar Zr/Y and Nb/Y values, respectively, 12.91–15.09 and 1.94–2.03 (Table 1; Fig. 5a). These coincide closely with those of the Averno 2 pumice fall deposit (Di Vito et al. 2011), erupted at about 5.2 ka (Fedele et al. 2011), but individual values of Zr and Nb are lower than Averno 2 values, and fall more closely within the range of Agnano crater pumice (de Vita et al. 1999), erupted at about 4.1 ka (Fedele et al. 2011). The Ta/Th ratio ranges from 0.75 to 0.87, similar to Averno, Astroni, and possibly Bacoli pumice compositions (de Vita et al. 1999; Di Vito et al. 2011; Fedele et al. 2011); no published Ta/Th bulk pumice analyses exist for the Agnano pumice fall deposit. La/Yb ratios in the BAI.06.03P1, BAI.06.03P3, and BAI.06.05P2 pumices values also coincide with Averno crater deposits (Fig. 5b), and with those of several other Flegrean Fields pumices, but not the pre-NYT or pre-Campanian Ignimbrite pumice compositions. Vesuvian pumices have wide ranging composition with higher Zr/Y and Nb/Y ratios overall and, in some cases, lower La/Yb than the Flegrean Fields pumices.

It is possible that the pumice could have been quarried from Averno crater, and then transported 1–2 km to the harbor sites; this would have been a direct route before the development of Mount Nuovo in 1538 (Di Vito et al. 1987). Transport from Agnano crater would have required a 4.5 km journey by oxcart to Puteoli, and an additional 3–4 km by road or sea to *Portus Baianus* and *Portus Iulius*. It is not yet clear whether the fine ash pozzolan (*pulvis*) also came from these deposits, or from poorly consolidated NYT deposits (Stanislao et al. 2011). The low-SiO_2 content of the pumice pozzolan and tuff coarse aggregates (Fig. 5b) reveals the strong loss in silicon that occurs during pozzolanic reaction and alteration in the seawater concrete environment; calcium content varies with development of cementitious phases. The pumice pozzolan has lost up to 20 wt% SiO_2, and about 30 wt% Na_2O+K_2O relative to the trachytic Averno pumice deposit (Di Vito et al. 2011), and both the Bacoli Tuff in the 2004 experimental reproduction and the *Baianus Sinus* tuff *caementa* have lost 5 to 10 wt% SiO_2 relative to the phonolitic-trachytic NYT (Orsi et al. 1992).

The trace element signatures validate ancient descriptions of sources of pyroclastic rock (Appendix 1). They provide a basis for further studies to identify original compositions of the pyroclastic rock that builders selected as pozzolanic materials for far distant concrete harbor installations. Even so, strong depletion of major elements in the pumice pozzolan suggests that pozzolanic dissolution of volcanic glass and precipitation of cementitious hydrates could disturb presumably immobile trace element concentrations relative to geological occurrences, especially as the phenocryst to glass ratio increases.

Discussion

Comparison with geologic occurrences of Al-tobermorite

Tobermorite with 11 Å interlayer spacing in basaltic tephra and lavas from hydrothermal environments has a wide range of aluminous compositions (Fig. 9; Supplemental Database 1). Alumina contents measured through microprobe analyses range between 3.16 to 6.30 wt% for tephra immersed in seawater (Jakobsson and Moore 1986; Aguirre et al. 1998), 3.96 to 4.20 wt% for amygdules in lavas in contact with hydrothermal fluids (Claringbull and Hey 1952; Livingstone 1988), and 0 to 3.31 wt%

for calc-silicate rocks in metamorphic skarn environments (Mitsuda and Taylor 1978; Henmi and Kusachi 1992; Maeshima et al. 2003). The Wessels Mine tobermorite has a nearly pure calcium-silicate-hydrate composition (Merlino et al. 2001; Hoffman and Armbruster 1997). Higher Na_2O and K_2O concentrations, 0.41 to 1.44 and 0.24 to 1.11 wt%, respectively, occur in crystals in the vesicles of basaltic volcanic ash altered in seawater (Jakobsson and Moore 1986; Aguirre et al. 1998), as compared with lower concentrations, 0 to 0.23 wt%, in tobermorite that formed in highly calcic skarn environments (Mitsuda and Taylor 1978; Henmi and Kusachi 1992; Maeshima et al. 2003).

In comparison, *Baianus Sinus* and *Portus Neronis* Al-tobermorites have even greater Al^{3+} substitution for Si^{4+}, with alumina contents of about 4 wt% and Al/(Si+Al) = 0.17 to 0.19. Calcium contents are in about the same range as pure tobermorite, about 33 to 35 wt% as compared with 37 wt% (Table 2), so the particularly low-silica contents, about 39 to 40 wt%, reflect pervasive alumina substitution. This is likely the result of saturation with respect to portlandite at pH > 12.7 and high Al^{3+} mobility (Massazza 1985). When the atoms per formula unit are calculated on the basis of 18[O,(OH)], (Si^{4+}+Al^{3+}) is about 5.80, compared with 6.00 for ideal tobermorite and 5.5 for the type locality of Al-tobermorite from Tobermory, Island of Skye (Livingstone 1988) (Table 2). This indicates that there is little or no Al^{3+} in octahedral coordination, in direct contrast with the ancient C-A-S-H, which has nearly identical Ca/(Si+Al) = 0.79 but both tetrahedrally and octahedrally coordinated aluminum (Fig. 6).

The charge induced by Al^{3+} substitution for Si^{4+} is balanced by Na^+ and K^+ interlayer cations in hydrothermal crystals (Taylor 1992; Mitsuda and Taylor 1978; Barnes and Scheetz 1991), alkali-activated high-temperature laboratory syntheses (Komarneni and Roy 1983; Komarneni and Tsuji 1989; Barnes and Scheetz 1991; Shaw et al. 2000; Sun et al. 2006; Houston et al. 2009) as well as the Roman seawater concrete syntheses, which contain 0.6 to 2.5 wt% Na_2O and 0.7 to 1.2 wt% K_2O. Calcium may also occur as an interlayer cation in the Roman crystals. In comparison, the average composition of C-A-S-H within the perimetral rim of a representative lime clast (Fig. 3) contains 1 to 2 at% Na and K; Mg, Fe, Ti, S, and Cl are not present in detectable concentrations. The water content of the Al-tobermorite crystals, about 11 to 12 wt%, is about the same as that in geologic occurrences, and may reflect sorption of water molecules in interlayer micropores (Tsuji et al. 1991), and possible charge compensation through substitution of OH^- for O^{2-}.

Silicon and aluminum bonding environments

Tetrahedral linkages across the silicate interlayer shown by the Q^3(1Al), Q^3(0Al), and Q^3(2Al) indicate that the *Baianus Sinus* Al-tobermorite has a double silicate-tetrahedra chain structure (Figs. 8a and 8c) (Komarneni et al. 1985; Sun et al. 2006; Houston et al. 2009), as in the geological occurrence of pure tobermorite described by Merlino et al. (2001). The pervasive tetrahedral cross-linkages, and the long silicate chain lengths indicated by a prominent Q^2(1Al) peak at 65.63 ppm (Fig. 8b) and low Ca/(Si+Al) ~ 0.8 indicate a high degree of polymerization and Si^{4+} binding energy. This typically produces strong cement paste in modern concretes (Komarneni et al. 1985; Sasaki et al. 1996; Sun et al. 2006). The wide interlayer spacing of the *Baianus Sinus* Al-tobermorite, 11.49 Å (Fig. 4) is similar to Al-tobermorite syntheses at 175 °C and ≥15% Al^{3+} substitution for Si^{4+} with 11.45 Å basal spacing (Diamond et al. 1966), and also at 90 to 190 °C, where the (002) interlayer spacing increases from 11.3 Å in pure tobermorite to 11.42 ± 0.019 at Al/(Al+Si) ≥ 0.15 largely as a result of Al-O bonds that are about 8–10% longer than Si-O bond lengths (Barnes and Scheetz 1991; Shannon 1976). Stable Al-tobermorites of the Earth's crust generally have interlayer cations that balance the charge induced by Al^{3+} replacement of Si^{4+} (Komarneni et al. 1985; Barnes and Scheetz 1991; Taylor 1992). The wide interlayer in the Roman crystals presumably provides cavities for Na^+ and K^+ cations derived from reaction between the alkali-rich volcanic ash and seawater-saturated lime, and contributes to charge balancing and stability (Komarneni et al. 1985; Tsuji et al. 1991; Taylor 1992).

Modern semicrystalline C-A-S-H typically has ^{IV}Al in bridging sites, Q^2(1Al) (e.g., Richardson et al. 1993). Al^{3+} substitution for Si^{4+} in C-A-S-H with low Ca/Si/Al = 0.85/1.00/0.15 produces a negative charge balance overall, and increased silanol binding capacity (Taylor et al. 2010; Richardson and Groves 1993). This encourages the irreversible binding of alkali cations in alkaline environments, and increased resistance to chemical attack compared with C-S-H (Hong and Glasser 2002), and may help explain the role of ^{IV}Al in the chemical stability of *Baianus Sinus* C-A-S-H. The presence of ^{VI}Al is usually associated with hydrotalcite, as in slag concretes (Richardson and Groves 1992; Richardson et al. 1993; Taylor et al. 2010). In the perimetral C-A-S-H zone of the *Baianus Sinus* relict lime clasts, however, the constant presence of silicon and absence of magnesium and iron (Fig. 3c), and the fine nanoscale distribution of ^{VI}Al in NEXAFS spectra (Fig. 6c) suggest that a secondary oxide phase with octahedral Al^{3+} is not present. Sun et al. (2006) find the maximum substitution for ^{IV}Al/(^{IV}Al+Si) in silicate chains at longer curing times is ~0.17, and that additional aluminum occurs in ^{V}Al and ^{V1}Al bonding environments. In the ancient C-A-S-H, ^{IV}Al may therefore reflect heterogeneous concentrations of aluminum, beyond average Al/(Al+Si) = 0.17 to 19 (Table 2, Fig. 3) Molecular dynamics simulations of tobermorite-like C-A-S-H predict that Al^{3+} substitution for Ca^{2+} in interlayer cavities produces rearrangement of water molecules and ^{VI}Al in octahedral coordination, which leads to additional silicate chain linkages with alkali earth elements that improve mechanical properties (Quomi et al. 2012). Such models may help explain the nanoscale ^{IV}Al and ^{VI}Al heterogeneity {Figs. 6c and 6d [C-A-S-H spectra (1), (2), (3)]} that appears to be an integral feature of the ancient C-A-S-H.

Thermal model of the *Baianus Sinus* breakwater

Estimated adiabatic time-temperature profiles (Fig. 10) are calculated in a model *Baianus Sinus* block with estimates of the original concrete mix design by mass (Appendix Table 1), submerged in the 14 to 26 °C seawater of Pozzuoli Bay (Damiani et al. 1987), with an initial 5 °C temperature increase from the sudden exothermic portlandite reaction, and heat evolved during hydration of C-A-S-H cementitious binder, with previously reported thermal and material properties of the volcanic rock, lime, and calcium-aluminate-cement paste (Appendix 1).

Concrete mix design. The original seawater concrete mix design of the harbor concretes has been previously described

as vol%, using empirical observations and the recommendation of a 1:2 volumetric ratio of lime:*pulvis* volcanic ash indicated by Vitruvius (Oleson et al. 2004, 2006; Brandon et al. 2008). Calculations of the relative proportions of geologic materials as weight percent (Appendix Table 1) use bulk mass densities of 1200 to 1400 kg/m^3 for the lithified facies of the NYT (Papakonstantinou et al. 2012), as an approximation or the Bacoli Tuff; 880 kg/m^3 for the dry lump quicklime (Brune 2011), calcined at about 900 °C; and 1000 to 1200 kg/m^3 for the loosely consolidated facies of the NYT (Papakonstantinou et al. 2012), a source of lightweight aggregate in modern structural concretes (de'Gennaro et al. 2005), which provides an approximation for the pumiceous ash pozzolan, possibly from the Averno 2 pumice fall deposit (Fig. 5). The mortar forms about 35 vol% of the BAI.06.03 concrete, and the tuff coarse aggregate about 65 vol% (Brandon et al. 2008). Before submersion in seawater this would have corresponded to dry unit weight of about 1105–1313 kg/m^3, composed of about 780 to 910 kg lithified pumiceous tuff, 83 to 96 kg dry quicklime, 242 to 307 kg pumiceous ash pozzolan (Appendix 1). The quicklime would have formed 6 to 9 wt% of the total mix. The measured unit weight of the BAI.06.03 drill core concrete, 1494 kg/m^3, results from hydration of quicklime to portlandite and the additional weight of the binding pozzolanic cementitious components, about 560 kg/m^3 for C-A-S-H (Appendix 1) plus Al-tobermorite, and chloride, sulfate, and zeolitic phases, and/or variations in the assumed weights and proportions of the raw materials.

Time-temperature profiles. Vitruvius observed that the "sudden saturation of lime (*calyx*), powdery ash (*pulvis*), and volcanic tuff (*tofus*) in an abundance of seawater" produced an exothermic reaction that "seethes with the latent heat in these substances" and causes them "to quickly assemble to gather thoroughly into excellent solid masses" (Appendix 1). This abrupt liberation of heat came from the nearly instantaneous reaction of lime with seawater to produce portlandite, $CaO+H_2O \rightarrow Ca(OH)_2$ (Hassibi 1999; Moropoulou et al. 2001). Reaction of portlandite with Flegrean ash produces various calcium silicate hydrates at low heats of hydration (Sersale and Orsini 1969), and it is this evolution of heat that should have produced measurable temperature increases in the ancient concrete installations. Based on point counts and petrographic analysis, the cementitious binder to volcanic aggregate ratio is about 3.15:1 (Vola et al. 2011b), and C-A-S-H hydration products are intimately associated with relicts of pumiceous pozzolan. To estimate maximum temperatures, C-A-S-H is approximated as forming the bulk of the binder, 86 wt% of the mortar or 37 wt% of the overall concrete. The heat evolution curve from 7 to 365 days hydration associated with formation of C-A-S-H uses that of an experimental concrete formulated with 40% by mass replacement of OPC with Italian volcanic pozzolan (Massazza 2002; see also Senhadji et al. 2012), the best available approximation to Vitruvius' 37 to 46% by mass ratio of ash pozzolan in the seawater mortar (Appendix Table 1).

The thermal model suggests maximum temperatures of 56 to 68 °C for Al-tobermorite specimens 0.85 m beneath the *pilae* surface, and 85 to 97 °C at the *pilae* center at 28 to 55 days hydration in 14 or 26 °C seawater, respectively (Fig. 10; Appendix Table 2). About two years after the installation of the concrete, the temperature of the *pilae* was the same as the seawater. The thermal diffusivity of the consolidating concrete was about 0.02 m^2/day, substantially less than conventional Portland cement concrete, about 0.096 m^2/day (Li 2007) and NIST mortars made with silica sand (Bentz et al. 2011). The *pilae* was constructed over several days, at least, and its upper surface likely projected above ancient sea levels (Brandon et al. 2008), suggesting lower temperatures than the model calculation. The proximity of the *pilae* to currently active fumaroles could have led to higher temperatures, but these conditions, as well as sea level fluctuations (Dvorak and Mastrolorenzo 1991; Morhange et al. 2006) and actual installation methods, are impossible to ascertain. The 2004 Roman seawater concrete reproduction at Brindisi harbor provides some insights, however. The 2 m^3 *pilae* was slightly warm to the touch 24 h after installation (Oleson et al. 2006). In 2009, five years after construction, it had not developed Al-tobermorite and the few relict lime clasts retained traces of portlandite (Jackson et al. 2012). The concrete mix used aged slaked lime, not quicklime, and Flegrean ash was mixed into a stiff seawater-lime putty before packing the mortar with tuff coarse aggregate in a wooden form (Oleson et al. 2006). It seems that this mixing procedure, the absence of relict lime clasts, and rapid loss of heat in the small structure produced obstacles to Al-tobermorite crystallization.

Comparison with hydration of ordinary Portland cement (OPC)

In OPC concretes, uncontrolled hydration at temperatures exceeding ~65 °C leads to the uptake of sulfate by developing C-S-H, which is subsequently expelled after cooling and aging to form deleterious ettringite in a mechanism called DEF for "delayed ettringite formation" (Taylor et al. 2001). The cement paste expands and debonds from aggregate, creating characteristic voids surrounding these particles, as described by Folliard et al. (2006, and references therein). The massive columns of bridge elements of the San Antonio, Texas, "Y", for example, suffer from severe DEF degradation and expansion that results from the small surface area of the structures compared to their volume, combined with use of undiluted OPC with no supplemental cementitious materials, and hot Texas temperatures >38 °C.

The massive concrete blocks of the Roman maritime constructions also have a very low surface to volume ratio, and a modest elevation in temperature occurred during hydration. However, there is little evidence for expansion or cracking at the micro- or macro-structural scales. Sulfate ions do not occur in the C-A-S-H dominated cementitious matrix, but rather are isolated in subspherical microstructures containing ettringite, as shown by high-resolution SEM-EDS maps of the *Portus Claudius* and *Portus Neronis* mortar fabrics (Jackson et al. 2012). Whereas elevated temperature during setting can be disastrous for structures made with OPC, this was apparently a benefit for ancient Roman concrete, as regards the crystallization of Al-tobermorite and, potentially, increased Al^{3+} mobility in high-pH interstitial fluids (Tagirov and Schott 2001) that bound chloride and sulfate in primary hydrocalumite and ettringite microstructures. Roman perspectives may therefore be beneficial for concreting in hot climates (Walker 1992).

Crystallization of Al-tobermorite

Most syntheses of Al-tobermorite rely on what can be considered pozzolanic reaction in a broad sense (Massazza 2004)—but with an external source of heat added to the experimental system. For example, reaction of CaO, SiO_2, and Al_2O_3 in experimental alkaline systems similar in composition to the hydrated lime clasts of the ancient seawater mortars produced C-A-S-H from which Al-tobermorite crystallized in a few days at 150 °C (Houston et al. 2009), and calcsilicate-alkoxide gel from which Al-tobermorite crystallized in 5 h at 240 °C (Shaw et al. 2000). The internal restructuring of a poorly crystalline C-A-S-H precursor at these high temperatures increased the periodicity of silicate chains in the **a-b** crystallographic plane and order of CaO layers in the **c** direction, producing a phase transformation to crystalline Al-tobermorite (Shaw et al. 2000). Alkali-activated syntheses at 80 to 85 °C, with amorphous silica and zeolite, have produced Al-tobermorite in weeks or months (Komarneni and Roy 1983; Komarneni et al. 1985). Twelve years after the 1963–1967 Surtsey eruption in Iceland, Al-tobermorite and an authigenic assemblage of zeolite and clay mineral (smectite) crystallized in the vesicles and altered vitric matrix of olivine alkali basalt tephra, at temperatures ranging from 70 to 150 °C, measured in 1979; the geothermal heat source was a subsurface dike swarm (Jakobsson and Moore 1986). Although Al-tobermorite occurred throughout the 150 m drill core, it was most abundant in the 105 °C submarine tuff. Petrographic analysis indicates that palagonitic tuffs from nearby Ellidaey and Bjarnarey islands developed a similar zeolite assemblage, but no Al-tobermorite, suggesting that ambient subaerial temperatures were not sufficient for crystallization (J.G. Moore, personal communication 2012).

The thermal model of the *Baianus Sinus* breakwater (Fig. 10) suggests two important differences regarding the crystallization of Al-tobermorite in the Roman pozzolanic seawater system, as compared with autoclaved laboratory syntheses and geothermal occurrences. First, the evolution of heat associated with hydration of quicklime and formation of C-A-S-H appears to have been sufficient, on its own, to produce the approximately 42 °C temperature rise required for Al-tobermorite crystallization at the specimen site. Second, the resulting maximum temperatures were low, 85 to 97 °C, compared with most experimental syntheses, and transitory, less than two years, compared with geothermal occurrences. The massive scale of the harbor structures, commonly >10 m^2 and 5 m thick, therefore seems to have been an important factor in producing sufficiently high temperature-time profiles in all the harbor structures. In addition, hydration in a seawater and alkali- and alumina-rich pozzolanic volcanic glass system, seems to have been critical to crystallization of Al-tobermorite in relict lime clasts. Crystallization of Al-tobermorite may have occurred quickly, perhaps over weeks or months, similar to 80 to 85 °C laboratory syntheses (Komarneni and Roy 1983; Komarneni et al. 1985), or a few years, as in the hydrothermal system at Surtsey volcano (Jakobsson and Moore 1986). Although reaction kinetics may have been slow at low temperatures (Barnes and Scheetz 1991; Shaw et al. 2000; Sun et al. 2006; Houston et al. 2009), they did not prevent Al-tobermorite crystallization in all the Mediterranean harbor concretes (Vola et al. 2011a; Stanislao et al. 2011; Jackson et al. 2012).

Conventional concretes rely on the short-lived reaction of OPC components to form C-S-H in a system of cement paste, and relatively inert sand and coarse aggregate. In principle, cement grains should continue to hydrate over time, but in most systems hydration is largely complete about one year after installation, since outer product phases armor the unhydrated clinker relic from further reaction with interstitial fluids (Richardson and Groves 1993). After the initial hydration process, there is little crystalline evolution of the C-S-H binder and portlandite, although chain lengths may increase in C-A-S-H of slag concretes (Taylor et al. 2010). Nowadays, natural and artificial pozzolans, such as volcanic tephra and fly ash, reduce the volume of kiln-fired cement and produce high ultimate strengths and durability even in seawater concrete environments (Massazza 2004; Thomas et al. 2011). These components continue to hydrate and form new aluminous cementitious phases long after initial OPC hydration (Mehta 1990; Massazza 2004), as interstitial phillipsite, for example, in the Roman seawater concrete (Vola et al. 2011a; Jackson et al. 2012). As conventional concretes age, however, the absence of even moderately elevated temperatures, low alkalinity, and low calcium and alumina solubility seems to prevent eventual nucleation of Al-tobermorite, either through topochemical reactions on C-A-S-H or through dissolution-precipitation mechanisms (Houston et al. 2009). In experimental Al-rich OPC pastes, the crystallization of Friedel's salt [$Ca_2Al(OH)_6(Cl,OH)\cdot 2H_2O$] and kuzelite (the mineral name of monosulfoaluminate, $3CaO\cdot Al_2O_3\cdot CaSO_4\cdot 12H_2O$), and related solid solution chloro- and sulfo-aluminate phases has been attributed to the binding of chloride and sulfate from the aqueous cement pore fluid at high pH with "aluminate" present in the paste to form AFm (aluminate-ferrite-monosubstituent calcium aluminum hydrate) phases (Birnin-Yauri and Glasser 1998). A somewhat similar process may occur in the ancient maritime concretes during hydration in seawater, where chloride and sulfate are sequestered in discrete crystalline hydrocalumite and ettringite microstructures in relict voids or along the perimeters of relict lime clasts (Jackson et al. 2012). In addition, sulfate may play an important role as a mineralizer in the reaction kinetics (Sauman 1972; Mostafa et al. 2009) of the ancient concrete.

Conventional OPC concrete structures rely on chemical inertia of the aggregate for durability and longevity. However, deleterious reactions of the aggregate have been recognized since the 1940s in large structures worldwide, and tremendous amounts are spent annually on research and development for preventive measures as well as concrete rehabilitation and replacement (Broekmans 2012). European requirements, for example, specify a maximum content of 3 kg Na_2O_{eq} per m^3 concrete (Na_2O_{eq} = Na_2O wt% + 0.658 K_2O wt%) to minimize the risk of alkali-silica gel expansions in concrete structures (Livesey 2009). In comparison, the Na_2O_{eq} of the ancient seawater concrete mix is substantially higher, about 17 to 26 kg/m^3, based only on Bacoli ash pozzolan in the mortar (Table 1 and Appendix Table 1). The present investigation of the ancient Roman maritime concretes thus suggests that, if certain prerequisites are fulfilled, the reactivity of alkali-rich pozzolanic aggregate can actually be a good thing, thus defining a stark contrast with the most common perception of aggregate reactivity being deleterious.

During pozzolanic reaction, dissolution of the highly alkaline trachytic Flegrean ash with lime apparently infused the centers

of partially dissolved portlandite clasts with silicon, alumina and alkali cations that mimic the chemical and temperature conditions of relatively low-temperature experimental syntheses of Al-tobermorite, produced with amorphous silica and zeolite (Komarneni and Roy 1983; Komarneni et al. 1985). Attack on the silicate framework of the volcanic glass by OH^- ions apparently releases K^+ and Na^+ into alkali-rich pore fluids that reduce calcium solubility, and increase alumina and alkali sorption into C-A-S-H—and Al-tobermorite—with low Ca/Si (Hong and Glasser 2002; Taylor 1997). In tests of the pozzolanic activity of numerous Italian natural volcanic pozzolans, the Bacoli ash combined the greatest amount of $Ca(OH)_2$ after 60 days hydration (Sersale and Orsini 1969; Costa and Massazza 1974). The ash contains about 8 wt% K_2O (Table 1), almost an order of magnitude greater than the other ashes, with the exception of Pozzolane Rosse from the Alban Hills volcanic district, which Romans specifically selected for the concretes of the imperial age monuments of Rome (Jackson et al. 2010). Although pozzolanic activity of the Italian volcanic pozzolans at early ages depends on specific surface area, at long ages it is determined by reactive silica and alumina (Costa and Massazza 1974), in which the depolymerization of highly potassic glass is apparently enhanced by weak SiO_2-Al_2O_3 bonds with alkalis. Experimental work by Hong and Glasser (2002) indicates that desorption of alkali cations from an alkali-enriched cementitious solid phase, with a lower Ca/Si limit of 0.85, in alkali-free water is reduced. This suggests a somewhat irreversible process of alkali sorption into the C-A-S-H of the ancient maritime concretes and their architectural counterparts in the Roman monuments (Jackson et al. 2010) that enhances the chemical stability of the cementitious composites.

Implications for pyroclastic rock concretes

One of the most important results to come from the investigation of relict lime clasts in ancient Roman seawater concrete is the identification of differences between crystalline Al-tobermorite and poorly crystalline C-A-S-H in the same cementitious microenvironment. These materials have nearly identical compositions, with Ca:Si:Al = 100 atomic ratios of about 43:47:10 (Figs. 3 and 9) and Ca/(Al+Si) = 0.79, but they bind Al^{3+} very differently. The Al-tobermorite has about 5.8 atoms per formula unit Si^{4+} + Al^{3+}, nearly identical to 6.00 atoms Si^{4+} for ideal tobermorite, suggesting that all aluminum occurs in tetrahedral sites. This is confirmed by STXM and NMR studies, which show Al^{3+} consistently in tetrahedral coordination with oxygen, where it substitutes for silicon in $Q^2(1Al)$, $Q^3(1Al)$, and $Q^3(2\ Al)$ chain and branching sites (Figs. 6 and 8). By contrast, C-A-S-H has Al^{3+} in both tetrahedral and octahedral coordination with oxygen, and strong heterogeneities at the 25 nm scale (Fig. 6); these indicate different roles for Al^{3+} in the poorly crystalline material. The coherent, compact fabrics of the Roman maritime concrete structures demonstrate that silicon and aluminum bonding environments in both the Al-tobermorite and the C-A-S-H are sufficiently stable, with only slight secondary alteration to calcite (Figs. 3 and 7), to have remained intact and robust during two thousand years' exposure to an aggressive maritime environment.

Al-tobermorite crystallization temperatures are constrained by the thermal model of the *Baianus Sinus pilae* to be 97 °C, and more likely in the range of 65 to 85 °C (Fig. 10). The short-lived temperature rise associated with heat evolved through the formation of C-A-S-H binder suggests that the crystals could have formed early in the history of the concrete. Reaction kinetics were undoubtedly complex, but the mineralizing action of alkali cations, mainly Na^+ and K^+ from the pumiceous ash pozzolan, and Na^+ and SO_4^{2-} from seawater may have had a beneficial effect. This is in direct contrast to modern concretes, where alkali cations and sulfate commonly have deleterious effects, and cause damaging secondary expansions that can eventually destroy cohesiveness and structural integrity. Although small quantities of Na^+ and K^+ were incorporated in the Al-tobermorite and perhaps in the C-A-S-H, as well, SO_4^{2-} was not. Instead, SO_4^{2-} and Cl^- were sequestered in primary hyrdocalumite and ettringite microstructures near the perimeters of the lime clasts resulting, perhaps, from the migration of these anions through the lime clast after hydration in seawater.

A firm confirmation of the origin of the pumiceous ash pozzolan as from "the vicinity of Baie and the territory of the municipalities around Mount Vesuvius" [Vitruvius, 30 BCE, (Appendix 1)] through trace element studies (Fig. 5) indicates that further experimental study of the pozzolanic properties of similar zeolitized, alkali-rich volcanic glasses with lime mixtures should provide important insights into durable and sustainable concrete designs for modern maritime structures. In addition, further investigations of dynamic cementitious systems in hydrothermally altered tephra deposits, such as that at Surtsey volcano, Iceland, should be considered as critical geological analogs for the very long behavior of pozzolanic concretes formulated with pyroclastic rock.

Roman concrete technologies of the first century BCE were designed to prolong the service life of seawater harbor installations (Appendix 1). They provide a proven model for the production of crystalline Al-tobermorite without kiln-fired cement, through a relatively low-temperature portlandite system infused with seawater and silicon, aluminum, sodium, and potassium cations from a pumiceous alkali- and alumina-rich Flegrean Fields pozzolan. Ongoing mineralogical studies are investigating the material properties of the Al-tobermorite, the precise provenance of the pumiceous pozzolan in maritime structures throughout the Mediterranean area, and characteristics of the ancient cementitious matrix and pore fabrics to evaluate their resistance to chlorine and sulfate attack. These studies will further clarify the reasons for the extraordinary longevity of the ancient seawater structures and provide predictions for the behavior of modern pozzolanic concretes.

Acknowledgments

This research was supported by Award No. KUS-l1-004021, from King Abdullah University of Science and Technology (KAUST) and the Loeb Classical Library Foundation at Harvard University. Data were acquired at beamlines 5.3.2.1, 5.3.2.2, and 12.2.2 at the Advanced Light Source at the Lawrence Berkeley Laboratories supported by the Director of the Office of Science, Department of Energy, under Contract No. DE-AC02-05CH11231, and the Advanced Nanofabrication Imaging and Characterization Laboratories at King Abdullah University of Science and Technology. We thank the ROMACONS drilling program: J.P. Oleson, C. Brandon, R. Hohlfelder, and CTG Italcementi researchers and staff, especially B. Zanga, in Bergamo, Italy; A.D. Kilcoyne and T. Tyliszczak at the 5.3.2.1, 5.3.2.2 beamlines; and S. Clark at the 12.2.2 beamline. T. Teague, D. Hernandez, B. Black, C. Hagen, and C. Kosso provided research support. We thank M. Sintubin, G. Sposito, P.-A. Itty, P. Brune, and J. Kirz for critical discussions, and the anonymous reviewers whose comments improved the manuscript. H.-R. Wenk acknowledges support

by NSF (EAR-0836402). The Berkeley Research Impact Initiative provided funds for Open Acess.

REFERENCES CITED

Aguirre, L., Dominguez-Bell, S., Morata, D., and Winke, O. (1998) An occurrence of tobermorite in tertiary basalts from Patagonia, Chile. Canadian Mineralogist, 36, 1149–1155.

Allen, A.J., Thomas, J.J., and Jennings, H.M. (2007) Composition and density of nanoscale calcium-silicate-hydrate in cement. Nature Materials, 6, 311–316.

Anthony, J.W., Bideaux, R.A., Bladh, K.W., and Nichols, M.C. (1995) Tobermorite, Handbook of Mineralogy. Volume II, Part 2: Silica, Silicates. Mineral Data Publishing, Tucson.

Balonis, M., and Glasser, F. (2009) The density of cement phases. Cement and Concrete Research, 39, 733–739.

Barnes, M.W., and Scheetz, B.E. (1991) The chemistry of Al-tobermorite and its coexisting phases at 175 °C. In B.E. Scheetz, A.G. Landers, I. Oder, and H. Jennings, Eds., Specialty cements with advanced properties, 179, 243–271. Material Research Society Symposium Proceedings, Warrendale, Pennsylvania.

Bentz, D.P., Peltz, M.A., Durán-Herrera, A., Valdez, P., and Juárez, C.A. (2011) Thermal properties of high-volume fly ash mortars and concretes. Journal of Building Physics, 34, 263–275.

Benzerara, K., Yoon, T.H., Tyliszczak, T. Constantz, B., Spormann, A.M., and Brown, G.E. Jr. (2004) Scanning transmission X-ray microscopy study of micro bialcalcification. Geobiology, 2, 249–259.

Birnin-Yauri, U.A., and Glasser, F.P. (1998) Friedel's salt, $Ca_2Al(OH)_6(Cl,OH)\times 2H_2O$: Its solid solutions and their role in chloride binding. Cement and Concrete Research, 28, 12, 1713–1723.

Brandon, C., Hohlfelder, R.L., and Oleson, J.P. (2008) The concrete construction of the Roman harbours of Baiae and Portus Iulius, Italy: The ROMACONS 2006 field season. International Journal of Nautical Archaeology, 37, 374–392.

Broekmans, M.A.T.M. (2012) Deleterious reactions of aggregate with alkalis in concrete. In M.A.T.M. Broekmans and H. Pöllmann, Eds., Applied Mineralogy of Cement and Concrete, 74, 279–364. Reviews in Mineralogy and Geochemistry, Mineralogical Society of America, Chantilly, Virginia.

Brune, P. (2011) The mechanics of imperial Roman concrete and the structural design of the Roman monuments. (Ph.D thesis), 413 p. University of Rochester, Rochester, New York. See also http://gh.carmeusegroup.com/files/files/downloads/SDS_carmeuse_CaO.pdf.

Brune, P., and Perucchio, R. (2012) Roman concrete vaulting in the Great Hall of Trajan's Markets: Structural evaluation. Journal of Architectural Engineering, 18, 332–340.

Civetta, L., Carluccio, E., Innocenti, F., Sbrana, A., and Taddeucci, G. (1991) Magma chamber evolution under the Phlegraean Fields during the last 10 ka: Trace element and isotope data. European Journal of Mineralogy, 3, 415–428.

Claringbull, G.F., and Hey, M. (1952) A re-examination of tobermorite. Mineralogical Magazine, 29, 960–962.

Costa, U., and Massazza, F. (1974) Factors influencing the reaction with lime of pozzolanas. Proceedings of the 6th International Congress on the Chemistry of Cement, III-6, 3–18. Moscow.

Damiani, V., Baudo, R., De Rosa, S., De Simone, R., Ferretti, O., Izzo, G., and Serena, F. (1987) A case study: Bay of Pozzuoli (Gulf of Naples, Italy). Hydrobiologia, 149, 201–211.

De Astis, G., Pappalardo, L., and Piochi, M. (2004) Procida volcanic history: New insights into the evolution of the Phlegraean Volcanic District (Campania region, Italy). Bulletin of Volcanology, 66, 622–641.

de'Gennaro, M., Cappelletti, P., Langella, A., Perrotta, A., and Scarpati, C. (2000) Genesis of zeolites in the Neapolitan Yellow Tuff: Geological, volcanological and mineralogical evidence. Contributions to Mineralogy and Petrology, 139, 17–35.

de'Gennaro, R., Cappelletti, P., Cerric, G., de'Gennaro, M., Dondi, M., and Langella, A. (2005) Neapolitan Yellow Tuff as raw material for lightweight aggregates in lightweight structural concrete production. Applied Clay Science, 28, 309–319.

de Vita, S., Orsi, G., Civetta, L., Carandente, A., D'Antonio, M., Deino, A., di Cesare, T., Di Vito, M.A., Fisher, R.V., Isaia, R., and others. (1999) The Agnano-Monte Spina eruption, 4100 years BP in the restless Campi Flegrei caldera, Italy. Journal of Volcanology and Geothermal Research, 91, 269–301.

Di Vito, M., Lirer, L., Mastrolorenzo, G., and Rolandi, R. (1987) The 1538 Monte Nuovo eruption (Campi Flegrei, Italy). Bulletin of Volcanology, 49, 608–615.

Di Vito, M.A., Arienzo, I., Braia, G., Civetta, L., D'Antonio, M., Di Renzo, V., and Orsi, G. (2011) The Averno 2 fissure eruption: a recent small-size explosive event at the Campi Flegrei Caldera (Italy). Bulletin of Volcanology, 73, 295–320.

Diamond, S., White, J.L., and Dolch, W.L. (1966) Effects of isomorphous substitution in hydrothermally-synthesized tobermorite. American Mineralogist, 51, 388–401.

Dvorak, J., and Mastrolorenzo, G. (1991) The mechanisms of recent vertical crustal movements in Campi Flegrei caldera, southern Italy. Geological Society of America Special Paper 263, Boulder, Colorado.

Fedele, L., Insinga, D.D., Calvert, A. T., Morra, V., Perrotta, A., and Scarpati, C. (2011) $^{40}Ar/^{39}Ar$ dating of tuff vents in the Campi Flegrei caldera (southern Italy): Toward a new chronostratigraphic reconstruction of the Holocene volcanic activity. Bulletin of Volcanology, 73, 1323–1336.

Folliard, K.J., Barborak, R., Drimalas, T., Lianxiang, D., Garber, S., Ideker, J., Ley, T., Williams, S., Juenger, M., Fournier, B., and Thomas, M.D.A. (2006) Preventing ASR/DEF in new concrete: Final report. Center for Transportation Research, University of Texas at Austin. Federal Highway Administration Report FHWA/TX-06/0-4085-5.

Giarimita, M.J., and Day, H.W. (1990) Error propagation in calculations of structural formulas. American Mineralogist, 75, 170–182.

Granger, F. (1931, reprint 2002) Vitruvius On Architecture, Books 1–5, 6–10. Loeb Classical Library Nos. 251, 280. Harvard University Press, Cambridge, Massachusetts.

Hassibi, H. (1999) An overview of lime slaking and factors that affect the process (2009 revision). Presentation to 3rd International Sorbalit Symposium, http://agtgroup.cl/mining/doc/OverviewLimeSlakingProcess.pdf.

Henmi, C., and Kusachi, I. (1992) Clinotobermorite, $Ca_5Si_6(O,OH)^{18}5H_2O$, a new mineral from Fuka, Okayama Prefecture, Japan. Mineralogical Magazine, 56, 353–358.

Hitchcock, A.P. (2011) aXis 2000, an IDL-based analytical package, date of retrieval 13 March 2013, http://unicorn.mcmaster.ca/aXis2000.html.

Hoffman, C., and Armbruster, T. (1997) Clinotobermorite, $Ca_5[Si_3O_8(OH)]^24H_2O$, a natural C-S-H(I) type cement mineral: Determination of the substructure. Zeitschrift für Kristallographie, 212, 864–873.

Hong, S.-Y., and Glasser, F.P. (2002) Alkali sorption by C-S-H and C-A-S-H gels Part II. Role of Alumina. Cement and Concrete Research, 32, 1101–1111.

Houston, J., Maxwell, R.S., and Carroll, S.A. (2009) Transformation of meta-stable calcium silicate hydrates to tobermorite: Reaction kinetics and molecular structure from XRD and NMR spectroscopy. Geochemical Transactions, 10, 1–14.

Jackson, M., and Kosso, C. (2013) *Scientia* in republican era stone and concrete masonry. In J. R. Evans, Ed., A Companion to the Archaeology of the Roman Republic, First Edition, p. 268–284. Blackwell, Oxford.

Jackson, M.D., Logan, J., Scheetz, B.E., Deocampo, D.M., Cawood, C.G., Marra, F., Vitti, M., and Ungaro, L. (2009) Assessment of material characteristics of ancient concretes, Grande Aula, Markets of Trajan, Rome. Journal of Archaeological Science, 36, 2481–2492.

Jackson, M., Deocampo, D., Marra, F., and Scheetz, B. (2010) Mid-Pleistocene volcanic ash in ancient Roman concretes. Geoarchaeology, 25, 36–74.

Jackson, M.D., Vola, G., Všianský, D., Oleson, J.P., Scheetz, B., Brandon, C., and Hohlfelder, R. (2012) Cement microstructures and durability in ancient Roman seawater concretes. In J. Valek, C. Groot, and J. Hughes, Eds., Historic Mortars. Characteristics and Tests, p. 49–76. Springer–RILEM, Berlin.

Jackson, M.D., Moon, J., Gotti, E., Kunz, M., Taylor, R., Emwas, A.-H., Meral, C., Guttmann, P., Levitz, P., Wenk, H.-R., and Monteiro, P.J.M. (2013) Material and elastic properties of Al-tobermorite in ancient Roman sea-water concrete. Journal of the American Ceramic Society, in press, DOI: 10.1111/jace.12407.

Jakobsson, S., and Moore, J.G. (1986) Hydrothermal minerals and alteration rates at Surtsey volcano, Iceland. Geological Society of America Bulletin, 97, 648–659.

Kato, Y., Shimizu, K., Matushita, N., Yoshida, T., Yoshida, H., Satsuma, A., and Hattori, T. (2001) Quantifications of aluminum coordinations in alumina and silica-alumina by Al K edge XANES. Physical Chemistry Chemical Physics, 3, 1925–1929.

Kilcoyne, A.L.D., Tyliszczak, T., Steele, W.F., Fakra, S., Hitchcock, P., Franck, K., Anderson, E., Harteneck, B., Rightor, E.G., Mitchell, G.E., and others. (2003) Interferometer-controlled scanning transmission X-ray microscopes at the Advanced Light Source. Journal of Synchrotron Radiation, 10, 125–136.

Kilcoyne, D., Ade, H., Attwood, D., Hitchcock, A., McKean, P., Mitchell, G., Monteiro, P., Tyliszczak, T., and Warwick, T. (2010) New scanning transmission X-ray microscope at the ALS for operation up to 2500 eV. Lawrence Berkeley National Laboratory lBNL3816E.

Komarneni, S., and Roy, D. (1983) Tobermorites: A new family of cation exchangers. Science, 221, 647–648.

Komarneni, S., and Tsuji, M. (1989) Selective cation exchange in substituted tobermorites. Journal of the American Ceramic Society, 12, 1668–1674.

Komarneni, S., Roy, R., Roy, D., Fyfe, C.A., Kennedy, G.J., Bothner-By, A.A., Dadok, J., and Chesnick, A.S. (1985) ^{27}Al and ^{29}Si magic angle spinning nuclear magnetic resonance spectroscopy of Al-substituted tobermorites. Journal of Material Science, 20, 4209–4214.

Komarneni, S., Breval, E., Miyake, M., and Roy, R. (1987) Cation-exchange properties of (Al+Na)-substituted synthetic tobermorites. Clays and Clay Minerals, 35, 385–390.

Krukowsky, S.T. (2010) Lime. In J.E. Kogel, N.C. Trivedi, and J.M. Barker, Eds., Industrial Minerals and Rocks: Commodities, markets, and users, p. 561–580. Society for Mining, Metallurgy, and Exploration, Littleton, Colorado.

Kunz, M., MacDowell, A.A., Caldwell, W.A., Cambie, D., Celestre, R.S., Domning, E.E., Duarte, R.M., Gleason, A.E., Glossinger, J.M., Kelez, N., and others. (2005) A beamline for high-pressure studies at the Advanced Light Source

with a superconducting bending magnet as the source. Journal of Synchroton Radiation, 12, 650–658.
Li, P. (2007) 3-D simulating analysis for thermal control during construction period of DAHUASHUI RCC Arch Dam. Proceedings of the 5th International Symposium on RCC Dams, p. 571–583, China Waterpower Press, Beijing.
Li, D., Bancroft, G.M., Fleet, M.E., Feng, X.H., and Pan, Y. (1995) Al *K*-edge XANES spectra of aluminosilicate minerals. American Mineralogist, 80, 432–440.
Livesey, P. (2009) Building Research Establishment Digest 330: Alkali silica reaction in concrete—the case for revision Part 1. Concrete, 43, 42–44.
Livingstone, A. (1988) Reyerite, tobermorite, calcian analcime and bytownite from amygdules in Skye basalt. Mineralogical Magazine, 52, 711–713.
Lothenbach, B., Scrivener, K., and Hooton, R.D. (2011) Supplementary cementitious materials. Cement and Concrete Research, 41, 217–229.
Lustrino, M., Martuarano, A., Morra, V., and Ricci, G. (2002) Volcanological and geochemical features of young pyroclastic levels (<12 Ka) in the urban area of Naples. Periodico di Mineralogia, 71, 241–253.
Maeshima, T., Noma, H., Sakiyama, M., and Mitsuda, T. (2003) Natural 1.1 and 1.4 nm tobermorites from Fuka, Okayama, Japan: Chemical analysis, cell dimensions, 29Si NMR and thermal behavior. Cement and Concrete Research, 33, 1515–1523.
Marra, F., Deocampo, D., Jackson, M., and Ventura, G. (2011) The Alban Hills and Monti Sabatini volcanic products used in ancient Roman masonry (Italy): An integrated stratigraphic, archaeological, environmental and geochemical approach. Earth Science Reviews, 108, 115–136.
Massazza, F. (1985) Concrete resistance to seawater and marine environment. Il Cemento, 1, 3–25.
——— (2002) Properties and applications of natural pozzolanas. In J. Bensted and P. Barnes, Eds., Structure and Performance of Cements, 2nd ed., p. 326–352. Taylor and Francis, London.
——— (2004) Pozzolana and pozzolanic cements. In P.C. Hewlett, Ed., Lea's Chemistry of Cement and Concrete, 4th ed., p. 471–632. Arnold, London.
McKeown, D.A., Waychunas, G.A., and Brown, G.E. Jr. (1985) EXAFS study of the coordination environment of aluminum in a series of silica-rich glasses and selected minerals within the sodium aluminosilicate system. Journal of Non-Crystalline Solids, 74, 349–375.
Mehta, P.K. (1990) Concrete in the Marine Environment. Elsevier, Oxford.
Merlino, S., Bonaccorsi, E., and Armbruster, T. (2001) The real structure of 11 Å tobermorite: Normal and anomalous forms, OD character and polytypic modifications. European Journal of Mineralogy, 13, 577–590.
Mindess, S., Young, J.F., and Darwin, D. (2003) Concrete. Pearson Education, Inc., Upper Saddle River, New Jersey.
Mitsuda, T., and Taylor, H.F.W. (1978) Normal and anomalous tobermorites. Mineralogical Magazine, 42, 229–235.
Morgan, G.B., and London, D. (2005) Effect of current density on the electron microprobe analysis of alkali aluminosilicate glasses. American Mineralogist, 90, 1131–1138.
Morhange, C., Marriner, N., Laborel, J., Todesco, M., and Oberlin, C. (2006) Rapid sea-level movements and noneruptive crustal deformations in the Phlegrean Fields caldera, Italy. Geology, 34, 93–96.
Moropoulou, A., Bakolas, A., and Aggelakopoulou, E. (2001) The effects of limestone characteristics and calcination temperature to the reactivity of the quicklime. Cement and Concrete Research, 31, 633–639.
Mostafa, N.Y., Shaltout, A.A., Omar, H., and Abo-El-Enein, S.A. (2009) Hydrothermal synthesis and characterization of aluminum and sulfate substituted 1.1 nm tobermorites. Journal of Alloys and Compounds, 467, 332–337.
Oleson, J.P., Brandon, C., Cramer, S.M., Cucitore, R., Gotti, E., and Hohlfelder, R.L. (2004) The ROMACONS Project: A contribution to the historical and engineering analysis of hydraulic concrete in Roman maritime structures. International Journal Nautical Archaeology, 33, 199–229.
Oleson, J.P., Bottalico, L., Brandon, C., Cucitore, R., Gotti, E., and Hohlfelder, R.L. (2006) Reproducing a Roman maritime structure with Vitruvian pozzolanic concrete. Journal of Roman Archaeology, 19, 29–52.
Orsi, G., D'Antonio, M., de Vita, S., and Gallo, G. (1992) The Neapolitan Yellow Tuff, a large-magnitude trachytic phreatoplinian eruption: Eruptive dynamics, magma withdrawal and caldera collapse. Journal of Volcanology and Geothermal Research, 53, 275–287.
Orsi, G., de Vita, S., and Di Vito, M. (1996) The restless, resurgent Campi Flegrei nested caldera (Italy): Constraints on its evolution and configuration. Journal of Volcanology and Geothermal Research, 74, 179–214.
Pabst, S., Wörner, G., Civetta, L., and Tesoro, R. (2008) Magma chamber evolution prior to the Campanian Ignimbrite and Neapolitan Yellow Tuff eruptions (Campi Flegrei, Italy). Bulletin of Volcanology, 70, 961–976.
Papakonstantinou, S., Pimentel, E., and Anagnostou, G. (2012) Analysis of artificial ground freezing in the Pari-Duomo platform tunnel of the Naples metro. In T. Benz and S. Nordal, Eds., Numerical Methods in Geotechnical Engineering, p. 281–284. Taylor and Francis, London.
Prince, K.C., Avaldi, L., Coreno, M., Camilloni, R., and De Simone, M. (1999) Vibrational structure of core to Rydberg state excitations of carbon dioxide and dinitrogen oxide. Journal of Physics B, 32, 2551–2567.
Quomi, M.J.A., Ulm, F.J., and Pellenq, R.J.-M. (2012) Evidence on the dual nature of aluminum in the calcium-silicate-hydrates based on atomistic simulations. Journal of the American Ceramic Society, 95, 1128–1137.
Rackham, H. (1952) Pliny: Natural history. Volume IX, Books 33–35. Loeb Classical Library No. 394, Harvard University Press, Cambridge, Massachusetts.
Richardson, I.G., and Groves, G.W. (1992) Microstructure and microanalysis of hardened ordinary Portland cement pastes. Journal of Materials Science, 27, 6204–6212.
——— (1993) The incorporation of minor and trace elements into calcium silicate hydrate (C-S-H) gel in hardened cement pastes. Cement and Concrete Research, 23, 131–138.
Richardson, I.G., Brough, A.R., Brydson, R., Groves, G.W., and Dobson, C.M. (1993) Location of aluminum in substituted calcium silicate hydrate (C-S-H) gels as determined by ^{29}Si and ^{27}Al NMR and EELS. Journal of the American Ceramic Society, 76, 2285–2288.
Rock-Color Chart Committee (1995) Rock-color chart with genuine Munsell colors. Eighth printing. Geological Society of America, Boulder, Colorado.
Sasaki, K., Masuda, T., Ishida, H., and Mitsuda, T. (1996) Structural degradation of tobermorite during vibratory milling. Journal of the American Ceramic Society, 79, 1569–1574.
Sauman, Z. (1972) Influence of SO_4^{2-} on the formation of 11 Å tobermorite. Proceedings of the 2nd International Symposium on Science and Research in Silicate Chemistry, p. 25–39, Research Institute of Building Materials, Brno.
Scarpati, C., Cole, P., and Perrotta, A. (1993) The Neapolitan Yellow Tuff—A large volume multiphase eruption from Campi Flegrei, Southern Italy. Bulletin of Volcanology, 55, 343–356.
Senhadji, Y., Escadeillas, G., Khelafi, H., Mouli, M., and Benosman, A.S. (2012) Evaluation of natural pozzolan as supplementary cementitious material. European Journal Environmental and Civil Engineering, 16, 77–96.
Sersale, R., and Orsini, P.G. (1969) Hydrated phases after reaction of lime with pozzolanic materials or with blast furnace slag. Proceedings of the 5th Symposium on the Chemistry of Cement, Tokyo, IV-7, 114–121.
Shannon, C.T. (1976) Revised effective ionic radii and systematic studies of interatomic distances in halides and chalcogenides. Acta Crystallographica, A32, 751–767.
Shaw, S., Clark, S.M., and Henderson, C.M.B. (2000) Hydrothermal formation of the calcium silicate hydrates, tobermorite ($Ca_5Si_6O_{16}(OH)_2 \cdot 4(H_2O)$ and xonolite ($Ca_6Si_6O_{17}(OH)_2$): An in situ synchroton study. Chemical Geology, 167, 129–140.
Skibsted, J., Jakobsen, H., and Hall, C. (1994) Direct observation of aluminum guest ions in the silicate phases of cement minerals by ^{27}Al MAS spectroscopy. Journal of the Chemical Society, 90, 2095–2098.
Snellings, R., Mertens, G., and Elsen, J. (2010) Calorimetric evolution of the early pozzolanic reaction of natural zeolites. Journal of Thermal Analysis and Calorimetry, 101, 97–105.
Stanislao, C., Rispoli, C., Vola, G., Cappelletti, P., Morra, V. and de'Gennaro, M. (2011) Contribution to the knowledge of ancient Roman seawater concretes: Phlegrean pozzolan adopted in the construction of the harbour at Soli-Pompeiopolis (Mersin, Turkey). Periodico di Mineralogia, 80, 471–488.
Sun, G.K., Young, J.F., and Kirkpatrick, R.J. (2006) The role of Al in C-S-H: NMR, XRD, and compositional results for precipitated samples. Cement and Concrete Research, 36, 18–29.
Tagirov, B., and Schott, J. (2001) Aluminum speciation in crystal fluids revisited. Geochimica et Cosmochimica Acta, 65, 3965–3992.
Taylor, H.F.W. (1992) Tobermorite, jennite, and cement gel. Zeitschrift für Kristallographie, 202, 41–50.
——— (1997) Cement Chemistry, 2nd ed. Thomas Telford, London.
Taylor, H.F.W., Famy, C., and Scrivener, K. (2001) Review: Delayed ettringite formation. Cement and Concrete Research, 31, 683–693.
Taylor, R., Richardson, I.G., and Brydson, R.M.D. (2010) Composition and microstructure of 20-year-old ordinary Portland cement–ground granulated blast-furnace slag blends containing 0 to 100% slag. Cement and Concrete Research, 40, 971–983.
Thomas, M.D.A., Bremner, T., and Scott, A.C.N. (2011) Actual and modelled performance in a tidal zone. Concrete International, 33, 23–28.
Tonarini, S., D'Antonio, M., Di Vito, M.A., Orsi, G., and Carandente, A. (2009) Geochemical and B-Sr-Nd isotopic evidence for mingling and mixing processes in the magmatic system that fed the Astroni volcano (4.1–3.8 ka) within the Campi Flegrei caldera (southern Italy). Lithos, 107, 135–151.
Tsuji, M., Komarneni, S., and Malla, P. (1991) Substituted tobermorites: ^{27}Al and ^{29}Si MASNMR, cation exchange, and water sorption studies. Journal of the American Ceramic Society, 74, 274–279.
Ukrainczyk, N., and Matusinovic, T. (2010) Thermal properties of hydrating calcium aluminate cement pastes. Cement and Concrete Research, 40, 128–137.
Vejmelková, E., Keppert, M., Rovnaníková, P., Keršner, Z., and Černy, R. (2012) Application of burnt clay shale as pozzolan addition to lime mortar. Cement and Concrete Composites, 34, 486–492.
Vola, G., Gotti, E., Brandon, C., Oleson, J.P., and Hohlfelder, R.L. (2011a) Chemical, mineralogical and petrographic characterization of Roman ancient hydraulic concretes cores from Santa Liberata, Italy, and Caesarea Palestinae,

Israel. Periodico di Mineralogia, 80, 317–338.
Vola, G., Stanislao, C., Rispoli, C., Morra, V., and de'Gennaro, M. (2011b) Petrographic quantitative analysis of pozzolanic mortars from ancient Roman marine concrete cores, drilled by ROMACONS team 2006–2009. Rendiconti Online Società Geologica Italiana, 11, 561–562 (with poster).
Walker, M.J. (1992) Concrete in hot climates. Proceedings of the Third International RILEM Conference on Concrete in Hot Climates. RILEM Proceedings 19. E and FN Spon Press, London.
Zhu, B. (1999) Thermal Stresses and Temperature Control of Mass Concrete. China Electric Power Press, Beijing.

Manuscript received January 28, 2013
Manuscript accepted May 7, 2013
Manuscript handled by Maarten Broekmans

Appendix 1: Unlocking the secrets of Al-tobermorite in Roman seawater concrete

—

Roman seawater concrete design and thermal analysis of the *Baianus Sinus pilae*

Romans' empirical observations of the seawater concretes recorded in Vitruvius' *de Architectura* (about 30 BCE) (Granger 1931) and Pliny's *Naturalis Historia* (23–79 CE) (Rackham 1952) provide essential information about mix design (Appendix Table 1) and installation practices (Oleson et al. 2004). New translations of Vitruvius' and Pliny's texts describe the raw materials of the maritime concrete:

> There is also a variety of powder [*pulveris*, fine-grained volcanic ash] which naturally effects an admirable result. It originates in the vicinity of Baiae and the territory of the municipalities around Mount Vesuvius. When mixed with lime (*calx*) and rubble (*caementum,* tuff coarse aggregate), it not only furnishes strength to other buildings, but also, when piers (*moles*) are built in the sea, they become solid underwater (*de Architectura* 2.6.1).

Pliny the Elder also described the *pulverem Puteolanus* volcanic ash:

> But other creations belong to the Earth itself. For who could marvel enough that on the hills of Puteoli there exists a dust (*pulvis*)—so named because it is the most insignificant part of the Earth—that, as soon as it comes into contact with the waves of the sea and is submerged, becomes a single stone mass, impregnable to the waves and every day stronger, especially if mixed with stones quarried at Cumae *(Naturalis Historia 35.166)*.

Vitruvius recommended a 1:2 lime to *pulvis* volcanic ash ratio by volume for seawater harbor mortars (Appendix Table 1):

> The concrete masonry (*structurae*) which is to be built in the water should be constructed in this way. Powder (*pulvis*) is to be brought from the region that runs from Cumae to the promontory of Minerva and mixed, in the mortar trough (*mortario*), two parts to one [of lime]... (*de Architectura* 5.12.2-3).

He described the sudden exothermic reaction that occurred when the lime-pyroclastic rock mixture was submerged in seawater:

> In that case, when unlike and unequal things [lime (*calx*), ash (*pulvis*), and tuff (*tofus*)] are collected and brought together into one arrangement, the hot lack of moisture suddenly comes into contact with an abundance of [sea]water, it seethes with the latent heat in the substances, and then vehemently affects these and quickly assembles to gather thoroughly into strong solid masses (*de Architectura* 2.6.4, Jackson and Kosso 2013).

The "seething" release of "latent heat" refers to the instantaneous liberation of heat that accompanied the reaction of quicklime (CaO) with seawater to produce calcium hydroxide [$Ca(OH)_2$], about 1155 kJ/kg of CaO at 25 °C (Krukowsky 2010; Brune 2011). The granular particles of relict lime in the mortar and their symmetrically dissolved perimeters (Fig. 3) suggest Romans may have mixed dry or damp pebble lime and ash in the mortar trough and submerged this in the flooded form with the tuff coarse aggregate, rather than producing a stiff lime paste and laboriously stirring in the ash (Oleson et al. 2006). The lime was likely quarried elsewhere and transported to the building site, since limestone does not crop out in the volcanic terrane of Pozzuoli Bay. The rapid consolidation of the concrete that Vitruvius described occurred through pozzolanic reaction of the calcium hydroxide, seawater, and volcanic ash to produce cementitious hydrates, mainly C-A-S-H (Vola et al. 2011, 2011b; Stanislao et al. 2011; Jackson et al. 2012).

Using the 1:2 ratio of lime:*pulvis* ash by volume indicated by Vitruvius and the unit weights of Appendix Table 1, the ratio by mass of ash pozzolan ranges from 0.37–0.44 (1*880:2*1200 = 880:2400 = 0.37 to 1*880:2*1000 = 880:2000 = 0.44). The quicklime would form about 27–31 wt% of the mortar formulation [880 kg/(2400+880) kg = 27 wt% to 880 kg/(2000+880) kg = 31

Appendix Table 1a. Proportions of geologic materials in the original mix of the *Baianus Sinus* seawater concrete

Raw materials of Roman seawater concrete (*de Architectura* 2.6.1, 5.12.2-3)	Unit weight (kg/m³)
calx	
dry lump quicklime	880*
pulvis	
Neapolitan Yellow Tuff, poorly consolidated, volcanic ash pozzolan	~1000–1200†
tofus or Flegrean Tuff	
Neapolitan Yellow Tuff, lithified tuff, decimeter-sized aggregate	~1200–1400†‡
BAI.06.03 concrete, from drill core	1494‡

* Krukowsky (2010), Brune (2011).
† Papakonstantinou et al. (2012).
‡ CTG Italcementi Laboratories.

Appendix Table 1b. Proportions of geologic materials in the original mix of the *Baianus Sinus* seawater concrete

Lime:*pulvis* ratio in dry seawater mortar mix		wt% dry mortar mix*		wt% dry concrete mix†		Unit weight dry concrete mix
by volume	by weight†	Lime	Ash	Lime	Ash	(kg/m³)
1:2‡	0.37–0.44	27–31	69–73	12–13	37–46	1050–1262
1:2.7§	0.27–0.33	21–25	75–79	8–11	37–44	1096–1229

* See explanation in text.
† Mortar forms about 55 vol%, and Flegrean tuff coarse aggregate about 65 vol% of the BAI.06.03 concrete (C. Brandon, personal communication, 2013).
‡ *de Architectura* 5.12.2-3 (Granger 2002; Oleson et al. 2004).
§ Oleson et al. (2006).

wt%]. The *pulvis* ash would form about 69–73 wt% of the mortar. Given these ratios, one cubic meter of the dry mortar mix would have contained about 238–273 kg dry quicklime, and about 690–876 kg ash pozzolan, depending on variations in the unit weights of the materials. A recent reproduction of the maritime concrete in 2004 suggests, however, that builders used a 1:2.7 lime:*pulvis* mix (Oleson et al. 2006), about the same volumetric ratio that Vitruvius recommended for concrete mortars on land (*de Architectura* 2.5.1). If so, dry quicklime would have formed about 21–25 wt% of the mortar. With the 1200–1400 kg/m^3 unit weight of the lithified NYT, this corresponds to: 540–630 kg tuff aggregate, 102–121 kg dry quicklime, 454–478 kg ash pozzolan for a unit weight of about 1096–1229 kg/m^3 for the dry concrete mix before submersion in seawater. The quicklime would form 8–11 wt% of the concrete.

A finite element analysis using the Structural Analysis Program for Temperature and Stress (SAPTS) program, designed to compute the evolution of temperatures associated with heats of hydration of cementitious components in large concrete dams (Zhu 1999; Li 2007), uses reasonable boundary conditions with measured and presumed material characteristics of the ancient concrete constituents to calculate time-temperature profiles in the massive *Baianus Sinus* breakwater (Fig. 9, Appendix Table 2). The approximate maximum adiabatic temperature is $\Theta = m_c Q_1/Cr$, where:

m_c Unit weight of cementitious hydrates in the concrete, 670 kg/m^3

Concrete components as estimated wt%:

48 wt% Neapolitan Yellow Tuff (NYT) – lithified tuff coarse aggregate (1300 kg/m^3),

45 wt% Cementitious hydrates (average, 2200 kg/m^3),

7 wt% Neapolitan Yellow Tuff (NYT) – ash pozzolan (1100 kg/m^3).

Notes:

1494 kg/m^3 unit weight of concrete from BAI.06.03 core (CTG Italcementi Laboratories, Bergamo, Italy),

1300 kg/m^3 unit weight of NYT lithified tuff aggregate (Papakonstantinou et al. 2012),

1100 kg/m^3 unit weight of unreacted NYT ash pozzolan (Papakonstantinou et al. 2012),

2200 kg/m^3 average unit weight of cementitious hydrates in the binding matrix (Mindess et al. 2003) (mainly C-A-S-H, < 10 wt% Al-tobermorite). This estimate is lower than 2622 kg/m^3 of C-S-H with Ca/Si=1.7 (Allen et al. 2007) and takes into account relict fine-grained pumiceous ash and pores in the cementitious binding matrix. 14Å tobermorite (piomberite) has density 2228 kg/m^3; portlandite has density 2251 kg/m^3 (Balonis and Glasser 2009).

55:45 measured volumetric ratio of mortar to tuff coarse aggregate, BAI.06.03 drill core (C. Brandon, personal communication, 2013).

3.15: 1 Ratio of cementitious binder:volcanic aggregate from point counts of thin sections (Vola et al. 2011b, this study). The binder is a complex microcrystalline pumiceous—C-A-S-H matrix, with abundant alteration to calcite in BAI06.03. The approximate unaltered mortar composition is estimated as:
1100/[3.15(2200) + 1100] = 14 wt% unreacted ash, and [3.15(2200)]/[3.15(2200) + 1100] = 86 wt% C-A-S-H matrix.

715 kg/m^3 weight of tuff coarse aggregate in one cubic meter of concrete [0.55 (1300 kg/m^3)],

779 kg/m^3 weight of mortar in one cubic meter of concrete (1494 – 715 = 779 kg/m^3),

670 kg/m^3 weight of cementitious hydrates in one cubic meter of concrete [0.86(779) = 670 kg/m^3],

109 kg/m^3 weight of unreacted ash (including lava lithic fragments) in one cubic meter of concrete [0.14(779) = 109 kg/m^3].

Q_1 Evolution of heat of hydration from a C-A-S-H cementitious component

In experimental studies of pozzolanic concretes, volcanic ash replaces up to 50 wt% of Portland cement (Massazza 2002; Senhadji et al. 2012), and progressively lower heat evolution accompanies increasing ash content. A phillipsite-rich specimen of the Neapolitan Yellow tuff produced a low 400 mW/kg exotherm after three hours reaction with hydrated lime (Snellings et al. 2010). The heat evolved for an experimental concrete formulated with 40 wt% Italian volcanic pozzolan replacement

Appendix Table 2. Changing adiabatic temperatures (Θ) over time, as as result of heat evolved through the formation of C-A-S-H, along the vertical center line of the 5.7 m thick *Baianus Sinus* block

Depth (m)	Temperature (°C)												
z	1	3	7	28	55	90	130	180	240	360	520	720	1080
Days hydration in 14 °C seawater, center line of *pilae*													
0.00	14	14	14	14	14	14	14	14	14	14	14	14	14
0.29	23	26	30	34	29	25	22	19	17	15	14	14	14
0.57	23	30	38	50	42	35	30	25	20	16	14	14	14
0.85	23	30	41	61	54	45	37	29	23	16	14	14	14
1.14	23	30	42	68	64	53	44	34	26	17	14	14	14
1.43	23	30	42	72	72	61	50	38	28	18	15	14	14
1.71	23	30	42	74	77	67	55	42	30	18	15	14	14
2.00	23	30	42	76	81	72	59	44	32	19	15	14	14
2.28	23	30	42	76	84	76	62	46	33	19	15	14	14
2.55	23	30	42	76	85	78	64	48	33	19	15	14	14
2.85	23	30	42	76	85	79	65	48	34	20	15	14	14
Days hydration in 26 °C seawater, center line of *pilae*													
0.00	26	26	26	26	26	26	26	26	26	26	26	26	26
0.29	35	38	42	46	41	37	34	31	29	27	26	26	26
0.57	35	42	50	62	54	47	42	37	32	28	26	26	26
0.85	35	42	53	73	66	57	49	41	35	28	26	26	26
1.14	35	42	54	80	76	65	56	46	38	29	26	26	26
1.43	35	42	54	84	84	73	62	50	40	30	27	26	26
1.71	35	42	54	86	89	79	67	54	42	30	27	26	26
2.00	35	42	54	88	93	84	71	56	44	31	27	26	26
2.28	35	42	54	88	96	88	74	58	45	31	27	26	26
2.55	35	42	54	88	97	90	76	60	45	31	27	26	26
2.85	35	42	54	88	97	91	77	60	46	32	27	26	26

Notes: z = 0 is the concrete surface and z = 2.85 is the body center.

of Portland cement at 7 days is 234 kJ/kg, at 28 days, 276 kJ/kg; at 90 days, 297 kJ/kg (Massazza 2002, table 13.17), and interpolating the curve to 360 days, 314 kJ/kg. This curve is used as a first approximation of the heat evolution of the seawater concrete (Q_1).

V_{pilae} Dimensions of the concrete block (*pilae*) breakwater

The measured dimensions of the *Baianus Sinus pilae* are 10 m ±30 cm on a side and 5.65 m tall, and submerged under 3.45 m seawater (Brandon et al. 2008). The model is a block 10 m^2 by 5.7 m high.

T_w 14–26 °C, seawater temperatures in the Bay of Pozzuoli

The *pilae* was cast in an underwater form, presumably flooded with seawater (Brandon et al. 2008). Annual variations in Pozzuoli Bay range from 14–26 °C (Damiani et al. 1987) but the proximity of the breakwater blocks to a presently active fumarole may have increased seawater temperatures. There is good circulation of seawater within the bay, however, and water temperatures at the time of drilling were not noticeably warm (J.P. Oleson, personal communication 2012). An accurate estimation of water depths at the time of construction is difficult because of the complex history of marine transgressions (sea-level rise) and non-eruptive uplifts (sea-level fall) associated with the active Flegrean Fields volcanic caldera over the past 2000 years (Morhange et al. 2006). Here, the model is simplified to a uniform boundary condition at the minimum and maximum annual temperature range.

T_o T_w + 5 °C, temperature of submerged hydrated lime-volcanic rock mix[1]

This is the approximate temperature several hours after the lime (*calx*), ash (*pulvis*), and tuff (*tofus*) concrete mix "suddenly comes into contact with an abundance of seawater" (*de Architectura* 2.6.4). During hydration of quicklime, two simultaneous phenomena occur: the temperature increases through exothermic reaction and the volume of the lime expands. Experimental results indicate that a variety of quicklimes fully hydrate to $Ca(OH)_2$ in a few minutes reaction time (Moroloupo et al. 2001). Immersion of 100 g of 18 °C quicklimes (with various particle sizes) into 400 mL coldwater (3.3 °C) raised water temperatures in 10 min 40–45 °C (Hassibi 1999). About 1155 kJ/kg heat is generated by lime hydration at 25 °C (Brune 2011).

The sudden immersion of the lime-volcanic rock mix in seawater and the immediate temperature rise that ensued (*de Architectura* 2.6.4) can be considered an initial temperature boundary condition: for about 10 wt% lime in the dry concrete mix (Appendix Table 1), 10% of the 40–45 °C temperature rise measured by Hassibi (1999) would have elevated temperatures in the submerged form approximately 5 °C, increasing the 14 °C seawater boundary condition to T_o = 19 °C, and 25 °C seawater boundary condition to T_o = 31 °C. If aged slaked lime were used in the concrete, the initial temperature rise in the *pilae* would be slightly lower, overall.

In this analysis, the heat of the concrete does not communicate with the underlying seafloor and volcanic substrate. All surfaces of the block maintain the same temperature, T_w, and there is a symmetrical distribution of temperatures within the block. Because the sediments and porous pyroclastic rock underlying the *pilae* were most likely water saturated, this seems a reasonable first approximation along the lower surface of the *pilae*, although its upper surface may have stood above sea level.

λ Thermal conductivity, 0.70 W/m°K for whole concrete

Notes:

0.49 W/m°K lithified NYT coarse aggregate (Papakonstantinou et al. 2012),

0.27 W/m°K volcanic ash pozzolan, NYT (Papakonstantinou et al. 2012),

0.98 W/m°K C-A-S-H, estimated from hydrated calcium aluminate cement paste (Ukrainczyk and Matusinovic 2010).

0.49 (0.48) + 0.27 (0.07) + 0.98 (0.45) = 0.70 W/m°K

C Specific heat capacity, 2.1 kJ/kg°K for whole concrete

Notes:

2.48 kJ/kg°K 3227 kJ/ m^3°K /1300 kg/m^3, coarse aggregate, lithified NYT (Papakonstantinou et al. 2012),

2.75 kJ/kg°K 3020 kJ/m^3°K (1100 kg/m^3), ash pozzolan, unconsolidated NYT (Papakonstantinou et al. 2012),

1.69 kJ/kg°K C-A-S-H, estimated from hydrated calcium aluminate cement paste (Ukrainczyk and Matusinovic 2010).

2.48 (0.48) + 2.75 (0.07) + 1.69 (0.45) = 2.1 kJ/kg°K

Estimated C of the ancient mortar is 0.95 kJ/kg°K, is similar to 0.85–0.96 kJ/kg°K for modern mortars with lime-pozzolan composite and fly ash (Vejmelková et al. 2012; Bentz et al. 2011).

ρ Unit weight of concrete in BAI.06.03 drill core, 1494 kg/m^3

CTG Italcementi Laboratories, Bergamo, Italy

α Thermal diffusivity, 2.2 X 10^{-7} m^2/s for the whole concrete block

$\alpha = \lambda/C\rho = 0.70$ W/m°K/[2.1 kJ/kg°K (1494 kg/m^3)] = 2.2×10^{-7} m^2/s

The exact position of the BAI.06.03 drill core is 1.2 m from the eastern face, 3 m from the southern face (Brandon et al. 2008), and the Al-tobermorite specimens studied here come from 0.83–0.85 m depth. The mesh size for the specimen temperature calculation is x = 1 m by y = 0.6 m by z = 0.285 m in the vicinity of the drill core. Calculations of Θ in chronological increments over three years suggest that the maximum temperature, 97 °C, at the center of the *pilae* immersed in 26 °C seawater, occurred at 28–90 days hydration (Appendix Table 2). For the *pilae* immersed in 14 °C seawater, the maximum temperature was 85 °C.